AIAA JOURNAL
Vol. 45, No. 7, July 2007

Dynamic Effects of a Radar Panel Mounted on a Truss Satellite

Armaghan Salehian,* T. Michael Seigler,† and Daniel J. Inman‡
Virginia Polytechnic Institute and State University, Blacksburg, Virginia 204060

DOI: 10.2514/1.23049

Presented here is an approach to find an equivalent continuum model of a radar truss structure with a radar panel mounted to the side. Kinetic and potential energy expressions of repeated truss elements are expanded in terms of the displacement components at its center. Two methods are proposed to account for the kinetic energy of the panel. The first considers the panel as a discrete set of point masses and the second method assumes a solid panel of constant density. Hamilton's principle is used to find the equations of motion for six coordinates of vibration for this structure and the original truss. For the truss-panel assembly, this results in two sets of partial differential equations resembling the extended Timoshenko beam equations. Both Euler–Bernoulli and Timoshenko formulations are derived and a finite element analysis is presented for comparison. The results are shown to be in good agreement with those of a finite element. The model demonstrates a significant change in the dynamic properties as a result of the panel. In particular, the longitudinal and torsional motions become coupled with the bending coordinates.

Nomenclature

A_L, A_d, A_b	=	cross-sectional area of the longerons, diagonals, and battens
$A^{(k)}$	=	cross-sectional area of member k
c	=	wave velocity
d_j	=	mode contribution factor
E_L, E_d, E_b	=	modulus of elasticity of the longerons, diagonals, and battens
$E^{(k)}$	=	modulus of elasticity of member k
f	=	frequency, Hz
H	=	coefficient matrix of the partial differential equation
I_1, I_2, I_3	=	moments of inertia of the panel
L_L, L_d, L_b	=	length of the longerons, diagonals, and battens
L_t	=	total length of the truss
$L^{(k)}$	=	length of member k
$l_i^{(k)}$	=	directional cosine of member k ($i = 1 \rightarrow 3$)
M	=	bending moment
m_p	=	mass of the panel distributed among the joints
m_{panel}	=	mass of the panel on a truss element
N	=	longitudinal force
Q	=	shear force
T	=	kinetic energy
t	=	time
U	=	potential energy
$\boldsymbol{U}_{1,i}, \boldsymbol{U}_{3,i}, \boldsymbol{\Omega}_i$	=	mode vectors
u_1, u_2, u_3	=	displacement components at the cross section in the x_1, x_2, and x_3 directions
$u_{1,0}, u_{2,0}, u_{3,0}$	=	displacement components evaluated at the center of the cross section
x_1, x_2, x_3	=	Cartesian coordinates
α	=	mode-shape parameter
$\varepsilon_{1,0}, \varepsilon_{2,0}, \varepsilon_{3,0}, \varepsilon_{12,0}, \varepsilon_{13,0}, \varepsilon_{23,0}$	=	strain components evaluated at the center of the cross section
$\varepsilon_{ij}^{(k)}$	=	strain components of member k
$\kappa_{2,0}, \kappa_{3,0}, \kappa_{t,0}$	=	curvatures evaluated at the center of the cross section
λ	=	wave length
$\rho L, \rho d, \rho b$	=	density of the longerons, diagonals, and battens
ϕ_1, ϕ_2, ϕ_3	=	rotational degrees of freedom of the cross section
ω	=	natural frequency, rad/s

I. Introduction

THE Innovative Space-Based Radar Antenna Technology (ISAT) program is intended to enable nonstop global surveillance of moving ground targets. These satellites (Fig. 1) are designed to operate in a medium Earth orbit (MEO) to provide improved coverage when compared with low-orbiting satellites. Such technology will require fewer satellites for global coverage and thus reduce the overall cost involved. However, a radar antenna operating at MEO must be so large that it cannot be launched on existing rockets. Space inflatable structures, which can be compressed into far smaller packages, provide one possible approach to placing large metrology systems in space. Inflatable structures have many advantages compared with mechanically deployed structures, such as lower weight, higher packaging efficiency, and easier maintenance. Such structures have a long history of use in aerospace applications, from the ECHO series of satellites in the 1960s to L'Garde's space-shuttle-launched Inflatable Antenna Experiment (IAE) in May 1996 [1]. Many proposed inflatable designs for space applications consist of trusslike or lattice structures because they are simple to construct and they have large stiffness-to-density ratios. An approach for studying the dynamic response of these structures has thus been a topic of importance. In this regard, two approaches that have received attention are the finite element method (FEM) and the continuum model. Although the FEM is a popular approach and sometimes an indispensable tool for analyzing complex systems, much of the mathematical structure is made inaccessible in the process of discretization. Moreover, FEM requires a significant amount of computing capacity to obtain reliable

Presented as Paper 2101 at the 47th AIAA/ASME/ASCE/AHS/ASC Structures, Structural Dynamics, and Materials Conference, Newport, RI, 1–4 May 2006; received 7 February 2006; revision received 21 February 2007; accepted for publication 8 March 2007.

*Ph.D. Candidate, Center of Intelligent Material Systems and Structures, Department of Mechanical Engineering, 300 Durham Hall, Mail Code 0261; armaghan@vt.edu. Member AIAA.

†Currently Assistant Professor, University of Kentucky, Department of Mechanical Engineering, 281 Ralph G. Anderson Building, Lexington, KY, 40506-0503; seigler@engr.uky.edu. Member AIAA.

‡G. R. Goodson Professor and Director, Center of Intelligent Material Systems and Structures, Department of Mechanical Engineering, 310 Durham Hall, Mail Code 0261; dinman@vt.edu. Fellow AIAA.

solutions when the number of truss members is large. Hence, the FEM approach naturally leads to large-order models with limited ability to include damping and may become too large for low-order control law designs. In dynamic analysis, the finite element analysis (FEA) may also produce more modes of vibration than are actually needed [2]. Alternatively, it was shown that the dynamics of a repeated lattice structure are approximated well by a continuum model having the same form as the standard beam equations [3]. This approach offers significantly more insight into the problems associated with structural and control design. Moreover, the existing methods for the design of control systems for distributed parameter models can be applied effectively if an appropriate continuum model of the structure can be found. For example, this approach opens the possibility of constructing input–output transfer functions between the sensing and actuation points [4], thus enabling the use of many well-established frequency-based control methods.

It was first shown in [5] that the forces and deformations of a small segment of the truss structure can be related to those of the continuum model to find the anisotropic effective rigidities (stretching, bending, and shearing) and the coupling between them. In [6,7], the nodal displacements of a truss structure were expanded in a Taylor series to derive the reduced mass and stiffness matrices of the structure; subsequently, the natural frequencies were found. A continuum model for beamlike lattice trusses with rectangular cross sections was developed in [8], in which the theory of [6,7] was modified to account for warping of the cross section. In a related work, continuum models for repetitive beamlike trusses with orthogonal tetrahedral configurations were found [9]. The authors of this work consider an asymmetric configuration in which the axial and shear effects are coupled. The fundamental static and free-vibration equations were then derived by defining the constitutive relations and applying the first law. In [10,11], the equivalent stiffness and mass matrices of truss elements with different configurations were found to compare the stiffness-to-density ratios. In another work, the governing partial differential equations (PDEs) for a two-dimensional lattice structure were derived using the force displacement relations and Newton's law [12]. The equivalent stiffness of a truss element was found by applying unit loads in different directions to find the corresponding static deformations. In [13], the effective elastic and dynamic characteristics of a repeating element were found to derive the reduced FEA mass and stiffness matrices and thus the natural frequencies and mode shapes. Lee [14] also developed a continuum model for a large periodic lattice beam using a spectral element approach. His method involved the derivation of the transfer matrices by assembling the spectral element matrices for each structural member within a lattice cell. The equivalent structural properties for two-dimensional lattice trusses were presented in this work. The equivalent beam properties of beamlike lattice trusses were determined in [15] from the concept of energy equivalence, in which the continuum stresses and strains are defined by their average values over the element. The method was applied to two-dimensional lattice elements. In a previous work, it was demonstrated that the governing equations of motion for a three-dimensional truss structure with a double-bay single-laced element configuration can be found by the use of Hamilton's principle [3].

In another work, the method of discrete homogenization was employed for continuous modeling of a quasi-repetitive lattice structure [16]. The method consists of assuming an asymptotic series expansion for the node displacements and the tension in the truss-bar members. The balance equations of nodal displacements and force displacement relations were developed by Taylor's expansion of finite differences. The solution was then found by numerical methods for a two-dimensional truss structure. A complete survey on the two classes of discrete field approaches is provided by [17]. These approaches are the micro method, by which one constructs and solves difference equation models (or difference-differential equations for mixed discrete-continuous systems), and the macro method, by which one constructs and solves the summation equation models (or summation-integral equations for mixed discrete-continuous systems). In both approaches, a set of governing difference equations can be obtained to find the continuum model [18–20].

The work shown in the previous literature is concerned with lattice structures with symmetric configurations. Of the cited work, only [9] considers an asymmetric configuration with orthogonal tetrahedral-lattice elements with more than four longerons. In the present work, we also focus on an asymmetric structure; however, the asymmetry is due to the addition of the radar panel mounted to the side of the truss rather than the configuration of the members. Because of the large mass of this panel (almost 12 times the mass of the original truss), its contribution to the dynamics of the system cannot be ignored. As will be demonstrated, the natural frequencies of the truss-panel structure are significantly different from those of the original truss (no panel). Moreover, the addition of the panel introduces coupling between the torsional and the longitudinal modes and the bending coordinates. This work demonstrates a method of determining an equivalent beam model for a truss-panel assembly. Also, the governing partial differential equations for both the truss and the truss-panel assembly are derived. It is shown that for the case of the truss with no panel, the bending equations resemble those of a conventional Timoshenko beam. Thus, the partial differential equation provides a simple tool to find equivalent properties of the continuum-beam model. The results of this work are thought to provide useful insight into the physical characteristics of these types of structures, as well as a simpler tool for analysis compared with the FEA. Finally, an important advantage of having a distributed parameter system is that many of the methods for the control design of such systems can be applied effectively for this structure. For example, we can use the transfer-function method by Yang and Tan [4], by which various control problems can be analyzed and solved in their transfer-function formulations.

II. Modeling

A schematic view of the structure studied here is shown in Fig. 1. Motivated by the current ISAT technology, the truss structure has a triangular cross section and is made of double-bay single-laced elements with pin joints. The fundamental truss element configuration and the bar members are shown in Fig. 2. The battens, diagonals, and the longerons shown in the figure are constructed of tubes; material and geometrical properties are provided in Table 1. Because the structure has a repeated pattern, it is only necessary to determine the kinetic and strain energy expressions of a single

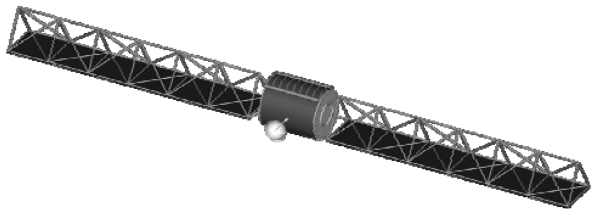

Fig. 1 Three-dimensional schematic of the ISAT.

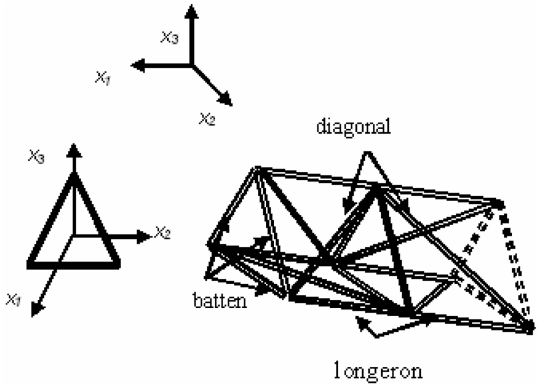

Fig. 2 Schematic view of a repeating element and reference coordinate system attached to midcross section.

Table 1 Material and geometrical properties of the truss

Truss properties	Values
Length of the radar antenna truss	300 m
Length of battens and longeron members	3 m
Modulus of elasticity of the batten, longeron, and diagonal	6.8948×10^4 Mpa
Mass density of the batten, longeron, and diagonal	1799.2 kg/m^3
Diameter of the diagonal and batten	25.4×10^{-3} m
Diameter of the longeron	76.2×10^{-3} m
Thickness of the diagonal and batten	0.508×10^{-3} m
Thickness of the longeron	1.016×10^{-3} m
Total mass of the radar panel	6000 kg
Mass of the truss	552 kg

element and then use Hamilton's principle to derive the governing partial differential equations for this structure. Two different formulations are considered: the Euler–Bernoulli and the Timoshenko equations. Some of the assumptions of Noor [7] are used to derive the strain energy of a repeated element in terms of the strain components evaluated at its center. This strain energy expression is then expanded in terms of the spatial derivatives of the displacement components. Furthermore, the kinetic energy of the truss element is written in terms of the time derivatives of the displacement components. Such displacement components are evaluated at the center of the element and are the same as those in the 1-D continuum-beam model. Two methods are presented to account for the kinetic energy of the panel. The first considers the panel as a discrete set of point masses distributed along the joints, and the second assumes a plate with a constant density. In the final section, numerical results for the natural frequencies of both the Timoshenko and Euler–Bernoulli continuum models are given and compared with those of a standard FEA for the purpose of validation.

A. Potential Energy

Considering a single truss element made of pin joints, as shown in Fig. 2, we can assume linear variations for displacement components in the plane of the cross section. Such displacement components (shown in Fig. 3) are [7]

$$\begin{aligned} u_1(x_1,x_2,x_3) &= u_{1,0}(x_1) - x_2\phi_3(x_1) + x_3\phi_2(x_1) \\ u_2(x_1,x_2,x_3) &= u_{2,0}(x_1) + x_2\varepsilon_{2,0}(x_1) + x_3\left\{-\phi_1(x_1) \right. \\ &\quad \left. + \tfrac{1}{2}[2\varepsilon_{23,0}(x_1)]\right\} \\ u_3(x_1,x_2,x_3) &= u_{3,0}(x_1) + x_2\left\{\phi_1(x_1) + \tfrac{1}{2}[2\varepsilon_{23,0}(x_1)]\right\} \\ &\quad + x_3\varepsilon_{3,0}(x_1) \end{aligned} \tag{1}$$

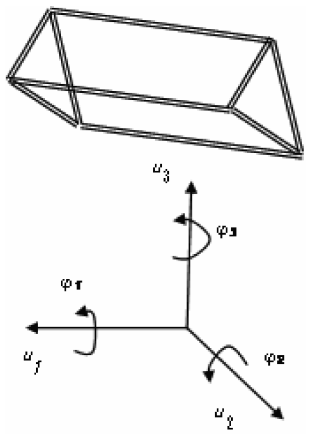

Fig. 3 Displacement components of the repeating element.

where $u_{1,0}$, $u_{2,0}$, and $u_{3,0}$ are the displacement components; ϕ_1, ϕ_2, and ϕ_3 are the rotations about the x_1, x_2, and x_3 axes; and $\varepsilon_{2,0}$, $\varepsilon_{23,0}$, and $\varepsilon_{3,0}$ are the strain components (due to the expansion of the cross section in the x_2 and x_3 directions and the shear strain), all evaluated at the center of the midcross section of the truss element. The Cartesian coordinates x_1, x_2, and x_3 are attached to the center of the midcross section, and x_1 is along the length of the truss. By making all the necessary assumptions with regard to a shear deformation type of beam, the compatibility conditions, and free local deformations [7], the strain components and their gradients can be found in terms of the strains evaluated at the center of the midcross section (see Appendix A).

Such strains are assumed to be the same as those of an equivalent continuum-beam model. Writing the strain components in terms of the spatial derivatives of the displacement components results in

$$\begin{aligned} U = L_L\Bigg[& c_1\left(\frac{\partial u_{1,0}}{\partial x_1}\right)^2 + c_2\left(\frac{\partial \phi_3}{\partial x_1}\right)^2 + c_3\left(\frac{\partial \phi_2}{\partial x_1}\right)^2 \\ & + c_4\left(\frac{\partial u_{2,0}}{\partial x_1} - \phi_3\right)^2 + c_5\left(\frac{\partial u_{3,0}}{\partial x_1} + \phi_2\right)^2 + c_6\left(\frac{\partial \phi_1}{\partial x_1}\right)^2\Bigg] \end{aligned} \tag{2}$$

where

$$\begin{aligned} c_1 &= 3A_LE_L, \qquad c_2 = c_3 = \frac{1}{2}A_LE_LL_b^2 \\ c_4 &= c_5 = \frac{6A_dA_LE_dE_LL_b^2L_dL_L}{A_dE_dL_dL_L^3 + 4A_LE_L(L_b^2 + L_L^2)^2} \\ c_6 &= \frac{A_dA_LE_dE_LL_b^4L_dL_L}{4(A_dE_dL_dL_L^3 + A_LE_L(L_b^2 + L_L^2)^2)} \end{aligned} \tag{3}$$

where the subscripts L, d, and b refer to the longerons, diagonals, and the battens, as shown in Fig. 2. The strain energy shown in Eq. (2) is valid for the case of a shearable model, which is the Timoshenko beam. A simpler equivalent is the Euler–Bernoulli beam model, in which the part of the strain energy that accounts for the shear deflection and the rotary inertia are ignored. Hence, for the strain energy of one repeating element,

$$\begin{aligned} U = L_L\Bigg[& c_1\left(\frac{\partial u_{1,0}}{\partial x_1}\right)^2 + c_2\left(\frac{\partial^2 u_{2,0}}{\partial x_1^2}\right)^2 + c_3\left(\frac{\partial^2 u_{3,0}}{\partial x_1^2}\right)^2 \\ & + c_6\left(\frac{\partial \phi_1}{\partial x_1}\right)^2\Bigg] \end{aligned} \tag{4}$$

B. Kinetic Energy

Because the radar panel mostly contains the electronic parts and is not made of a homogenous material, its elastic nature is complicated. Therefore, in our formulation, the strain energy stored in the panel is ignored and the panel segments mounted on each element are modeled as an additional mass. It should be noted that in the actual design, there is no connection between panels mounted on adjacent elements. To account for the kinetic energy of the panel, two different methods are used. In the first, the panel segments attached to each of the truss elements are modeled as a collection of point masses distributed among the bottom joints, and in the second model they are modeled as solid plates with constant density.

1. Point-Mass Model

We assume that the mass of the panel is distributed equally among the joints of the bottom face, as shown in Fig. 4. The kinetic energy of the truss-panel element can be found in terms of the time derivative of the displacement components at the center of the midcross section (for a complete derivation see Appendix B).

The expression for the kinetic energy of the truss-panel assembly for this model is

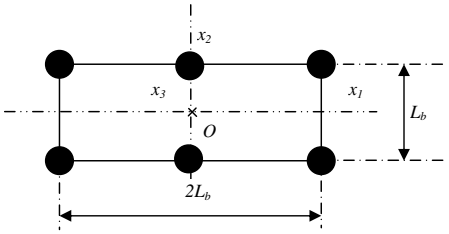

Fig. 4 Panel modeled as point masses.

$$T = 3(A_bL_b\rho_b + A_dL_d\rho_d + A_LL_L\rho_L)\left[\left(\frac{\partial u_{1,0}}{\partial t}\right)^2 + \left(\frac{\partial u_{2,0}}{\partial t}\right)^2 + \left(\frac{\partial u_{3,0}}{\partial t}\right)^2\right] + \frac{L_b^2(A_bL_b\rho_b + A_dL_d\rho_d + 2A_LL_L\rho_L)}{4} \times \left[2\left(\frac{\partial \phi_1}{\partial t}\right)^2 + \left(\frac{\partial \phi_2}{\partial t}\right)^2 + \left(\frac{\partial \phi_3}{\partial t}\right)^2\right] + m_p\left[\left(\frac{\partial u_{3,0}}{\partial t}\right)^2 + \left(\frac{\partial u_{1,0}}{\partial t}\right)^2 + \left(\frac{\partial u_{2,0}}{\partial t}\right)^2 + \frac{\sqrt{3}}{3}L_b\frac{\partial u_{2,0}}{\partial t}\frac{\partial \phi_1}{\partial t}\right] + m_p\left(-4\frac{\sqrt{3}}{3}L_b\frac{\partial u_{1,0}}{\partial t}\frac{\partial \phi_2}{\partial t} + \frac{L_b^2}{12}\left[4\left(\frac{\partial \phi_1}{\partial t}\right)^2 + \left(\frac{\partial \phi_2}{\partial t}\right)^2 + 3\left(\frac{\partial \phi_3}{\partial t}\right)^2\right]\right) \tag{5}$$

Note that the rotational components of the cross section (Φ_2 and Φ_3) are also included and they account for the rotary inertia effects. A simpler model can be derived by ignoring this effect, which will result in an Euler–Bernoulli model; the kinetic energy is

$$T = [3(A_bL_b\rho_b + A_dL_d\rho_d + A_LL_L\rho_L) + m_p]\left[\left(\frac{\partial u_{1,0}}{\partial t}\right)^2 + \left(\frac{\partial u_{2,0}}{\partial t}\right)^2 + \left(\frac{\partial u_{3,0}}{\partial t}\right)^2\right] + \left(\frac{L_b^2(A_bL_b\rho_b + A_dL_d\rho_d + 2A_LL_L\rho_L)}{2} + m_p\frac{L_b^2}{3}\right) \times \left(\frac{\partial \phi_1}{\partial t}\right)^2 + m_p\left(\frac{\sqrt{3}}{3}L_b\frac{\partial u_{2,0}}{\partial t}\frac{\partial \phi_1}{\partial t}\right) \tag{6}$$

2. Plate Model

Figure 5 shows the top and side views of the part of the element with the panel attached. Modeling each segment of the radar panel as a plate, the kinetic energy of the truss-panel assembly element can be found in terms of the displacement components of the midcross section, which again are the same as those of a continuum-beam model (see Appendix B for complete derivations).

$$T = 3(A_bL_b\rho_b + A_dL_d\rho_d + A_LL_L\rho_L)\left[\left(\frac{\partial u_{1,0}}{\partial t}\right)^2 + \left(\frac{\partial u_{2,0}}{\partial t}\right)^2 + \left(\frac{\partial u_{3,0}}{\partial t}\right)^2\right] + \frac{L_b^2(A_bL_b\rho_b + A_dL_d\rho_d + 2A_LL_L\rho_L)}{4} \times \left[2\left(\frac{\partial \phi_1}{\partial t}\right)^2 + \left(\frac{\partial \phi_2}{\partial t}\right)^2 + \left(\frac{\partial \phi_3}{\partial t}\right)^2\right] + \frac{m_{\text{panel}}}{2}\left[\left(\frac{\partial u_{1,0}}{\partial t}\right)^2 + \left(\frac{\partial u_{2,0}}{\partial t}\right)^2 + \left(\frac{\partial u_{3,0}}{\partial t}\right)^2\right] + \frac{1}{2}I_1\left(\frac{\partial \phi_1}{\partial t}\right)^2 + \frac{1}{2}I_2\left(\frac{\partial \phi_2}{\partial t}\right)^2 + \frac{1}{2}I_3\left(\frac{\partial \phi_3}{\partial t}\right)^2 + \frac{L_bm_{\text{panel}}}{2\sqrt{3}}\left(\frac{\partial u_{2,0}}{\partial t}\frac{\partial \phi_1}{\partial t} - \frac{\partial u_{1,0}}{\partial t}\frac{\partial \phi_2}{\partial t}\right) + \frac{1}{24}L_b^2m_{\text{panel}}\left[\left(\frac{\partial \phi_1}{\partial t}\right)^2 + \left(\frac{\partial \phi_2}{\partial t}\right)^2\right] \tag{7}$$

where m_{panel} is the mass of the radar panel on each truss element, as shown in Fig. 5. The moments of inertia I_1, I_2, and I_3 are measured around axes x_1, x_2, and x_3 and can be simply written as

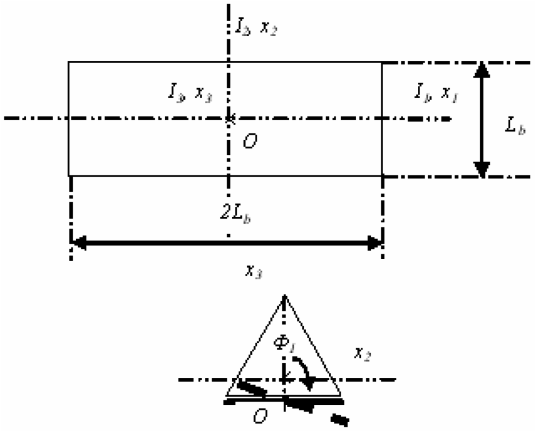

Fig. 5 Schematic view of the cross section of the ISAT structure (truss and radar panel).

$$I_1 = \frac{m_{\text{panel}}L_b^2}{12} \qquad I_2 = \frac{m_{\text{panel}}L_b^2}{3} \qquad I_3 = \frac{5m_{\text{panel}}L_b^2}{12} \tag{8}$$

An equivalent Euler–Bernoulli beam can be found by ignoring the effects of the rotary inertia for this model. The kinetic energy for this model is

$$T = 3(A_bL_b\rho_b + A_dL_d\rho_d + A_LL_L\rho_L)\left[\left(\frac{\partial u_{1,0}}{\partial t}\right)^2 + \left(\frac{\partial u_{2,0}}{\partial t}\right)^2 + \left(\frac{\partial u_{3,0}}{\partial t}\right)^2\right] + \frac{L_b^2(A_bL_b\rho_b + A_dL_d\rho_d + 2A_LL_L\rho_L)}{4} \times \left[2\left(\frac{\partial \phi_1}{\partial t}\right)^2\right] + \frac{1}{2}I_1\left(\frac{\partial \phi_1}{\partial t}\right)^2 + \frac{L_bm_{\text{panel}}}{2\sqrt{3}}\left(\frac{\partial u_{2,0}}{\partial t}\frac{\partial \phi_1}{\partial t}\right) + \frac{1}{24}L_b^2m_{\text{panel}}\left[\left(\frac{\partial \phi_1}{\partial t}\right)^2\right] + \frac{m_{\text{panel}}}{2}\left[\left(\frac{\partial u_{1,0}}{\partial t}\right)^2 + \left(\frac{\partial u_{2,0}}{\partial t}\right)^2 + \left(\frac{\partial u_{3,0}}{\partial t}\right)^2\right] \tag{9}$$

For the case of the original truss with no panel, the kinetic energy expression of the Timoshenko model reduces to

$$T = 3(A_bL_b\rho_b + A_dL_d\rho_d + A_LL_L\rho_L)\left[\left(\frac{\partial u_{1,0}}{\partial t}\right)^2 + \left(\frac{\partial u_{2,0}}{\partial t}\right)^2 + \left(\frac{\partial u_{3,0}}{\partial t}\right)^2\right] + \frac{L_b^2(A_bL_b\rho_b + A_dL_d\rho_d + 2A_LL_L\rho_L)}{4} \times \left[2\left(\frac{\partial \phi_1}{\partial t}\right)^2 + \left(\frac{\partial \phi_2}{\partial t}\right)^2 + \left(\frac{\partial \phi_3}{\partial t}\right)^2\right] \tag{10}$$

Similarly, for the original truss and the Euler–Bernoulli model, we get

$$T = 3(A_bL_b\rho_b + A_dL_d\rho_d + A_LL_L\rho_L)\left[\left(\frac{\partial u_{1,0}}{\partial t}\right)^2 + \left(\frac{\partial u_{2,0}}{\partial t}\right)^2 + \left(\frac{\partial u_{3,0}}{\partial t}\right)^2\right] + \left(\frac{L_b^2(A_bL_b\rho_b + A_dL_d\rho_d + 2A_LL_L\rho_L)}{2}\right)\left(\frac{\partial \phi_1}{\partial t}\right)^2 \tag{11}$$

C. Equations of Motion

Having the kinetic and strain energy expressions for an element, we will now employ Hamilton's principle to derive the governing partial differential equations of motion (see Appendix C for a complete derivation). These equations are presented here for the truss-panel assembly and original truss, using both Timoshenko and Euler–Bernoulli formulations.

1. Point-Mass Model

The equations of motion along the six coordinates of vibrations $u_{1,0}$, $u_{2,0}$, $u_{3,0}$, ϕ_1, ϕ_2, and ϕ_3 (longitudinal, two bending coordinates, torsional, and rotations of the cross section) are presented in this section. Note that the displacement components depend on x_1 only and are the same as those of the one-dimensional equivalent continuum-beam model. It will be shown that these equations decouple into two sets of coordinates. For the case of a Timoshenko-type beam, the equations of motion along the $u_{1,0}$, $u_{3,0}$, and ϕ_2 coordinates for this model can be found as follows:

$$\begin{cases} -2\sqrt{3}L_b m_p \frac{\partial^2 u_{1,0}}{\partial t^2} + 12c_5 L_L\left(\frac{\partial u_{3,0}}{\partial x_1} + \phi_2\right) + \left[3L_b^2(A_b L_b \rho_b + A_d L_d \rho_d + 2A_L L_L \rho_L) + L_b^2 m_p\right]\frac{\partial^2 \phi_2}{\partial t^2} - 12c_3 L_L \frac{\partial^2 \phi_2}{\partial x_1^2} = 0 \\ [3(A_b L_b \rho_b + A_d L_d \rho_d + A_L L_L \rho_L) + m_p]\frac{\partial^2 u_{3,0}}{\partial t^2} - c_5 L_L \frac{\partial^2 u_{3,0}}{\partial x_1^2} - c_5 L_L \frac{\partial \phi_2}{\partial x_1} = 0 \\ -[m_p + 3(A_b L_b \rho_b + A_d L_d \rho_d + A_L L_L \rho_L)]\frac{\partial^2 u_{1,0}}{\partial t^2} + c_1 L_L \frac{\partial^2 u_{1,0}}{\partial x_1^2} + \frac{\sqrt{3}}{6} L_b m_p \frac{\partial^2 \phi_2}{\partial t^2} = 0 \end{cases} \tag{12}$$

and for the three other coordinates $u_{2,0}$, Φ_1, and Φ_3, we get

$$\begin{cases} [6m_p + 18(A_b L_b \rho_b + A_d L_d \rho_d + A_L L_L \rho_L)]\frac{\partial^2 u_{2,0}}{\partial t^2} + \sqrt{3}L_b m_p \frac{\partial^2 \phi_1}{\partial t^2} + 6L_L c_4\left(\frac{\partial \phi_3}{\partial x_1} - \frac{\partial^2 u_{2,0}}{\partial x_1^2}\right) = 0 \\ \sqrt{3}L_b m_p \frac{\partial^2 u_{2,0}}{\partial t^2} + \left[3L_b^2(A_b L_b \rho_b + A_d L_d \rho_d + 2A_L L_L \rho_L) + 2L_b^2 m_p\right]\frac{\partial^2 \phi_1}{\partial t^2} - 6c_6 L_L \frac{\partial^2 \phi_1}{\partial x_1^2} = 0 \\ [L_b^2(A_b L_b \rho_b + A_d L_d \rho_d + 2A_L L_L \rho_L) + L_b^2 m_p]\frac{\partial^2 \phi_3}{\partial t^2} - 4L_L c_2 \frac{\partial^2 \phi_3}{\partial x_1^2} + 4c_4 L_L\left(\phi_3 - \frac{\partial u_{2,0}}{\partial x_1}\right) = 0 \end{cases} \tag{13}$$

2. Plate Model

In a similar manner, the Timoshenko equivalent model can be found for the case in which the radar panel is modeled as a plate. The equations of motion along three coordinates of vibrations $u_{1,0}$, $u_{3,0}$, and ϕ_2 for this case are

$$\begin{cases} -[6m_{\text{panel}} + 36(A_b L_b \rho_b + A_d L_d \rho_d + A_L L_L \rho_L)]\frac{\partial^2 u_{1,0}}{\partial t^2} + 12L_L C_1 \frac{\partial^2 u_{1,0}}{\partial x_1^2} + \sqrt{3}L_b m_{\text{panel}} \frac{\partial^2 \phi_2}{\partial t^2} = 0 \\ -\sqrt{3}L_b m_{\text{panel}} \frac{\partial^2 u_{1,0}}{\partial t^2} + 12L_L C_5\left(\frac{\partial u_{3,0}}{\partial x_1} + \phi_2\right) + 3\left[L_b^2(A_b L_b \rho_b + A_d L_d \rho_d + 2A_L L_L \rho_L) + \frac{5L_b^2 m_{\text{panel}}}{6}\right]\frac{\partial^2 \phi_2}{\partial t^2} - 12L_L C_3 \frac{\partial^2 \phi_2}{\partial x_1^2} = 0 \\ [6(A_b L_b \rho_b + A_d L_d \rho_d + A_L L_L \rho_L) + m_{\text{panel}}]\frac{\partial^2 u_{3,0}}{\partial t^2} - 2C_5 L_L\left(\frac{\partial^2 u_{3,0}}{\partial x_1^2} + \frac{\partial \phi_2}{\partial x_1}\right) = 0 \end{cases} \tag{14}$$

and for the other three coordinates $u_{2,0}$, Φ_1, and Φ_3, we have

$$\begin{cases} 6[6(A_b L_b \rho_b + A_d L_d \rho_d + A_L L_L \rho_L) + m_{\text{panel}}]\frac{\partial^2 u_{2,0}}{\partial t^2} - 12C_4 L_L \frac{\partial^2 u_{2,0}}{\partial x_1^2} + \sqrt{3}L_b m_{\text{panel}} \frac{\partial^2 \phi_1}{\partial t^2} + 12C_4 L_L \frac{\partial \phi_3}{\partial x_1} = 0 \\ 2\sqrt{3}L_b m_{\text{panel}} \frac{\partial^2 u_{2,0}}{\partial t^2} + \left(12\left[I_1 + L_b^2(A_b L_b \rho_b + A_d L_d \rho_d + 2A_L L_L \rho_L)\right] + L_b^2 m_{\text{panel}}\right)\frac{\partial^2 \phi_1}{\partial t^2} - 24C_6 L_L \frac{\partial^2 \phi_1}{\partial x_1^2} = 0 \\ -\left(I_3 + \frac{L_b^2(A_b L_b \rho_b + A_d L_d \rho_d + 2A_L L_L \rho_L)}{2}\right)\frac{\partial^2 \phi_3}{\partial t^2} + 2L_L C_2 \frac{\partial^2 \phi_3}{\partial x_1^2} + 2C_4 L_L\left(\frac{\partial u_{2,0}}{\partial x_1} - \phi_3\right) = 0 \end{cases} \tag{15}$$

As previously mentioned, each of the three coordinates of vibration $u_{2,0}$, Φ_1, and Φ_3 and $u_{1,0}$, Φ_2, and $u_{3,0}$ are coupled in the form of a PDE. These equations resemble those of an extended Timoshenko beam; which is a more general beam theory in which the longitudinal displacement is coupled to bending [12]. As a result of the panel, there is a coupling between the torsional or longitudinal vibrations and the bending coordinates. For the case of a truss with no panel, these torsional and longitudinal vibrations will be decoupled from the bending coordinates and the bending equations will have a form similar to a conventional Timoshenko beam (Salehian et. al. [3]). Moreover, by including the panel, the similarity between the equations for two bending coordinates along the x_2 and x_3 axes is lost, whereas these equations are identical for the original truss (for the configuration of the diagonal members shown in Fig. 2).

The equations of motion for the original truss (no panel) can be found in a manner similar to the previous derivation. The Φ_2 and $u_{3,0}$ coordinates are

$$\begin{cases} 3(A_b L_b \rho_b + A_d L_d \rho_d + A_L L_L \rho_L)\frac{\partial^2 u_{3,0}}{\partial t^2} - c_5 L_L\left(\frac{\partial^2 u_{3,0}}{\partial x_1^2} + \frac{\partial \phi_2}{\partial x_1}\right) = 0 \\ 3L_b^2(A_b L_b \rho_b + A_d L_d \rho_d + 2A_L L_L \rho_L)\frac{\partial^2 \phi_2}{\partial t^2} - 12c_3 L_L \frac{\partial^2 \phi_2}{\partial x_1^2} + 12c_5 L_L\left(\frac{\partial u_{3,0}}{\partial x_1} + \phi_2\right) = 0 \end{cases} \tag{16}$$

and the equations for the $u_{2,0}$ and Φ_3 coordinates are

$$\begin{cases} 3(A_b L_b \rho_b + A_d L_d \rho_d + A_L L_L \rho_L)\frac{\partial^2 u_{2,0}}{\partial t^2} - c_4 L_L\left(\frac{\partial^2 u_{2,0}}{\partial x_1^2} - \frac{\partial \phi_3}{\partial x_1}\right) = 0 \\ -3L_b^2(A_b L_b \rho_b + A_d L_d \rho_d + 2A_L L_L \rho_L)\frac{\partial^2 \phi_3}{\partial t^2} + 12c_2 L_L \frac{\partial^2 \phi_3}{\partial x_1^2} + 12c_4 L_L\left(\frac{\partial u_{2,0}}{\partial x_1} - \phi_3\right) = 0 \end{cases} \tag{17}$$

It should be noted that for the pattern of the diagonal members shown in Fig. 2, the coefficients c_2 and c_3 are identical, as are c_4 and c_5. As a result, it is obvious from Eqs. (16) and (17) that for this structure, the equations are identical for two bending coordinates u_2 and u_3. Also note that there is a sign difference for the rotation of the cross-sectional terms ϕ_2 and ϕ_3 in these equations. This is simply the result of the sign convention in Fig. 3 and will not impose any difference in the final solution. Solving for $\partial\phi_2/\partial x$ and $\partial\phi_3/\partial x$ from the first set of equations in Eqs. (16) and (17), taking an additional derivative with respect to the spatial variable x_1 from the second equation in Eqs. (16) and (17), and making the substitution

for $\partial\phi_2/\partial x$ and $\partial\phi_3/\partial x$, we find the decoupled bending equations of motion as follows:

$$\begin{aligned}\eta\frac{\partial^4 u_{2,0}}{\partial t^4}+\alpha\frac{\partial^4 u_{2,0}}{\partial x^4}+\gamma\frac{\partial^2 u_{2,0}}{\partial t^2}+\xi\frac{\partial^4 u_{2,0}}{\partial t^2\partial x^2}=0\\ \eta\frac{\partial^4 u_{3,0}}{\partial t^4}+\alpha\frac{\partial^4 u_{3,0}}{\partial x^4}+\gamma\frac{\partial^2 u_{3,0}}{\partial t^2}+\xi\frac{\partial^4 u_{3,0}}{\partial t^2\partial x^2}=0\end{aligned} \tag{18}$$

where

$$\begin{aligned}\eta&=\frac{(A_bL_b\rho_b+A_dL_d\rho_d+2A_LL_L\rho_L)(A_bL_b\rho_b+A_dL_d\rho_d+A_LL_L\rho_L)}{(A_LE_L+A_bE_b+A_dE_d)}\\ \alpha&=\frac{4A_dA_L^2E_dE_L^2L_b^2L_dL_L^3}{[A_dE_dL_dL_L^3+4A_LE_L(L_b^2+L_L^2)^2](A_LE_L+A_bE_b+A_dE_d)}\\ \gamma&=\frac{24A_dE_dL_dL_L^2A_LE_L(A_bL_b\rho_b+A_dL_d\rho_d+A_LL_L\rho_L)}{[A_dE_dL_dL_L^3+4A_LE_L(L_b^2+L_L^2)^2](A_LE_L+A_bE_b+A_dE_d)}\\ \xi&=-\frac{2A_dA_LE_dE_LL_b^2L_dL_L^2(A_bL_b\rho_b+A_dL_d\rho_d+2A_LL_L\rho_L)}{[A_dE_dL_dL_L^3+4A_LE_L(L_b^2+L_L^2)^2](A_LE_L+A_bE_b+A_dE_d)}\\ &\quad-\frac{2(A_bL_b\rho_b+A_dL_d\rho_d+A_LL_L\rho_L)A_LE_LL_L}{(A_LE_L+A_bE_b+A_dE_d)}\end{aligned} \tag{19}$$

Equation (18) is similar to the Timoshenko beam and identical for both bending equations $u_{2,0}$ and $u_{3,0}$. This similarity is a result of the diagonal pattern (Fig. 2) in which the intersection points of the diagonal members on each side of the truss lie on different longerons. If these intersection points were to coincide on the same longeron member, the similarity between the two bending equations in Eq. (18) would be lost. The torsional and longitudinal equations of motion for the original truss are similar to those of a bar:

$$\begin{aligned}\left(\frac{L_b^2(A_bL_b\rho_b+A_dL_d\rho_d+2A_LL_L\rho_L)}{2}\right)\frac{\partial^2\phi_1}{\partial t^2}-c_6L_L\frac{\partial^2\phi_1}{\partial x_1^2}=0\\ 3(A_bL_b\rho_b+A_dL_d\rho_d+A_LL_L\rho_L)\frac{\partial^2 u_{1,0}}{\partial t^2}-c_1L_L\frac{\partial^2 u_{1,0}}{\partial x_1^2}=0\end{aligned} \tag{20}$$

Again, a simpler form of all of the preceding equations can be derived by ignoring the effects of rotary inertia (i.e., by excluding the rotations of the cross sections Φ_2 and Φ_3 in the kinetic energy terms). For the shear strain components, we could assume that

$$\varepsilon_{12,0}=\varepsilon_{13,0}=\varepsilon_{23,0}=0 \tag{21}$$

Using these assumptions, the Euler–Bernoulli equations of motion for this structure and the point-mass model are

$$\begin{aligned}&[3(A_bL_b\rho_b+A_dL_d\rho_d+A_LL_L\rho_L)+2m_p]\frac{\partial^2 u_{1,0}}{\partial t^2}\\ &\quad-3A_LE_LL_L\frac{\partial^2 u_{1,0}}{\partial x_1^2}=0\\ &2[3(A_bL_b\rho_b+A_dL_d\rho_d+A_LL_L\rho_L)+2m_p]\frac{\partial^2 u_{3,0}}{\partial t^2}\\ &\quad+A_LE_LL_b^2L_L\frac{\partial^4 u_{3,0}}{\partial x_1^4}=0\\ &-2L_b(3A_bL_b\rho_b+3A_dL_d\rho_d+6A_LL_L\rho_L+4m_p)\frac{\partial^2\phi_1}{\partial t^2}\\ &\quad+\frac{3A_dA_LE_dE_LL_b^3L_L^2L_d}{A_dE_dL_L^3L_d+A_LE_LL_d^4}\frac{\partial^2\phi_1}{\partial x_1^2}-4\sqrt{3}m_p\frac{\partial^2 u_{2,0}}{\partial t^2}=0\\ &4m_p\left(\frac{\sqrt{3}}{2}L_b\frac{\partial^2\phi_1}{\partial t^2}+3\frac{\partial^2 u_{2,0}}{\partial t^2}\right)+3\Bigg[6(A_bL_b\rho_b+A_dL_d\rho_d\\ &\quad+A_LL_L\rho_L)\frac{\partial^2 u_{2,0}}{\partial t^2}+A_LE_LL_b^2L_L\frac{\partial^4 u_{2,0}}{\partial x_1^4}\Bigg]=0\end{aligned} \tag{22}$$

For the plate model, the corresponding equations are

$$\begin{aligned}&[6(A_bL_b\rho_b+A_dL_d\rho_d+A_LL_L\rho_L)+m_{\text{panel}}]\frac{\partial^2 u_{1,0}}{\partial t^2}\\ &\quad-6A_LE_LL_L\frac{\partial^2 u_{1,0}}{\partial x_1^2}=0\\ &[6(A_bL_b\rho_b+A_dL_d\rho_d+A_LL_L\rho_L)+m_{\text{panel}}]\frac{\partial^2 u_{3,0}}{\partial t^2}\\ &\quad+A_LE_LL_b^2L_L\frac{\partial^4 u_{3,0}}{\partial x_1^4}=0\\ &m_{\text{panel}}\left(\sqrt{3}L_b\frac{\partial^2\phi_1}{\partial t^2}+6\frac{\partial^2 u_{2,0}}{\partial t^2}\right)+6\Bigg[6(A_bL_b\rho_b+A_dL_d\rho_d\\ &\quad+A_LL_L\rho_L)\frac{\partial^2 u_{2,0}}{\partial t^2}+A_LE_LL_b^2L_L\frac{\partial^4 u_{2,0}}{\partial x_1^4}\Bigg]=0\\ &L_b\left(A_bL_b\rho_b+A_dL_d\rho_d+2A_LL_L\rho_L+\frac{m_{\text{panel}}}{6}\right)\frac{\partial^2\phi_1}{\partial t^2}\\ &\quad-\frac{A_dA_LE_dE_LL_b^3L_L^2L_d}{2(A_dE_dL_L^3L_d+A_LE_LL_d^4)}\frac{\partial^2\phi_1}{\partial x_1^2}+\frac{\sqrt{3}m_{\text{panel}}}{6}\frac{\partial^2 u_{2,0}}{\partial t^2}=0\end{aligned} \tag{23}$$

As shown in these equations, the rotations of the cross section do not appear in the Euler–Bernoulli formulation. The rotational components are dependent variables and they are simply the slopes of the beam in different bending directions. Also, bending in the x_3 direction (i.e., perpendicular to the panel surface) is decoupled from other coordinates of vibration in both kinetic energy models. This bending coordinate and the longitudinal vibrations remain identical for the two kinetic energy models. This is expected, because the rotary inertia terms are the only terms that are accounted for differently in these two kinetic energy models, and they are expressed in terms of the coordinates Φ_2 and Φ_3. Because these coordinates are ignored in the Euler–Bernoulli formulation (dependent variable), the equations for the two kinetic energy models remain the same.

D. PDE Solution

Following the approach used in [12] and assuming a harmonic solution for the coupled coordinates of vibrations (for example, $u_{1,0}$, $u_{3,0}$, and Φ_2), we have

$$\left.\begin{aligned}u_{1,0}&=U_1e^{\alpha x}e^{i\omega t}\\ u_{3,0}&=U_3e^{\alpha x}e^{i\omega t}\\ \phi_2&=\Omega e^{\alpha x}e^{i\omega t}\end{aligned}\right\}\Rightarrow\begin{Bmatrix}u_{1,0}\\ u_{3,0}\\ \phi_2\end{Bmatrix}=\begin{Bmatrix}U_1\\ U_3\\ \Omega\end{Bmatrix}e^{\alpha x}e^{i\omega t} \tag{24}$$

where U_1, U_3, and Ω are the amplitudes of vibration. By substituting Eq. (24) into Eq. (12), we get the following eigenvalue problem:

$$\begin{bmatrix}-a_5\omega^2 & a_3\alpha & a_3+a_4\alpha^2-a_1\omega^2\\ 0 & -a_3\alpha^2-a_2\omega^2 & -a_3\alpha\\ \underbrace{a_6\alpha^2-a_2\omega^2}_{H} & 0 & -a_5\omega^2\end{bmatrix}\begin{Bmatrix}U_1\\ U_3\\ \Omega\end{Bmatrix}=0 \tag{25}$$

where

$$\begin{aligned}a_1&=2L_b^2[3(A_bL_b\rho_b+A_dL_d\rho_d+2A_LL_L\rho_L)+m_p]\\ a_2&=24[3(A_bL_b\rho_b+A_dL_d\rho_d+A_LL_L\rho_L)+m_p]\\ a_3&=\frac{144A_dA_LE_dE_LL_b^2L_dL_L^2}{A_dE_dL_dL_L^3+4A_LE_L(L_b^2+L_L^2)^2}\qquad a_4=-12A_LE_LL_b^2L_L\\ a_5&=-4\sqrt{3}m_pL_b\qquad a_6=-72A_LE_LL_L\end{aligned} \tag{26}$$

For a nontrivial solution, the determinant of matrix H should vanish, that is,

$$\det(H) = 0 \Rightarrow K_1\alpha^6 + K_2\alpha^4 + K_3\alpha^2 + K_4 = 0 \tag{27}$$

where

$$\begin{gathered} K_1 = a_3a_4a_6 \qquad K_2 = (-a_2a_3a_4 - a_1a_3a_6 + a_2a_4a_6)\omega^2 \\ K_3 = a_2a_3a_6\omega^2 + (a_1a_2a_3 - a_2^2a_4 - a_3a_5^2 - a_1a_2a_6)\omega^4 \\ K_4 = -a_2^2a_3\omega^4 + (a_1a_2^2 - a_2a_5^2)\omega^6 \end{gathered} \tag{28}$$

The preceding equation is a cubic polynomial in α^2, and the roots of this polynomial can be found in terms of the natural frequencies ω. We then get six roots of α_i for each natural frequency ω. The solution of the mode vectors can be expressed in the form

$$\begin{gathered} \boldsymbol{U}_{1,i} = \begin{vmatrix} a_3\alpha_i & a_3 + a_4\alpha_i^2 - a_1\omega^2 \\ -a_3\alpha_i^2 - a_2\omega^2 & -a_3\alpha_i \end{vmatrix} = a_3a_4\alpha_i^4 + a_2a_3\omega^2 \\ - a_1a_3\alpha_i^2\omega^2 + a_2a_4\alpha_i^2\omega^2 - a_1a_2\omega^4 \\ \boldsymbol{U}_{3,i} = -\begin{vmatrix} -a_5\omega^2 & a_3 + a_4\alpha_i^2 - a_1\omega^2 \\ 0 & -a_3\alpha_i \end{vmatrix} = -a_3a_5\alpha_i\omega^2 \\ \boldsymbol{\Omega}_i = \begin{vmatrix} -a_5\omega^2 & a_3\alpha_i \\ 0 & -a_3\alpha_i^2 - a_2\omega^2 \end{vmatrix} = a_3a_5\alpha_i^2\omega^2 + a_2a_5\omega^4 \end{gathered} \tag{29}$$

The subscript $i(1 \rightarrow 6)$ denotes each of the six roots of α_i for each frequency ω. The free-vibration solution can be expanded in terms of the mode vectors and natural frequencies by

$$\begin{Bmatrix} u_{1,0}(x,t) \\ u_{3,0}(x,t) \\ \phi_2(x,t) \end{Bmatrix} = \sum_{j=1}^{6} d_j \begin{Bmatrix} U_{1,j} \\ U_{3,j} \\ \Omega_j \end{Bmatrix} e^{\alpha_j x} e^{i\omega t} \tag{30}$$

in which the six constants d_j are found from the boundary conditions. The boundary conditions for this structure are free–free and can be expressed as

$$\begin{bmatrix} N(0,t) \\ Q_{x_3}(0,t) \\ M_{x_2}(0,t) \end{bmatrix} = \begin{bmatrix} N(L_t,t) \\ Q_{x_3}(L_t,t) \\ M_{x_2}(L_t,t) \end{bmatrix} = \begin{bmatrix} 0 \\ 0 \\ 0 \end{bmatrix} \tag{31}$$

where Q_{x_3} and M_{x_2} are the shear force in the x_3 direction and the bending moment around the x_2 axis. Using the relation for the strain energy, Eq. (2), the stiffness matrix for an element can be found and the force displacement relation for an element can be written as

$$\begin{bmatrix} N \\ Q_{x_2} \\ Q_{x_3} \\ M_{x_3} \\ M_{x_2} \\ M_{x_1} \end{bmatrix} = \underbrace{\begin{bmatrix} c_1 & 0 & 0 & 0 & 0 & 0 \\ 0 & c_2 & 0 & 0 & 0 & 0 \\ 0 & 0 & c_3 & 0 & 0 & 0 \\ 0 & 0 & 0 & c_4 & 0 & 0 \\ 0 & 0 & 0 & 0 & c_5 & 0 \\ 0 & 0 & 0 & 0 & 0 & c_6 \end{bmatrix}}_{K} \begin{bmatrix} \frac{\partial u_{1,0}}{\partial x} \\ -\phi_3 + \frac{\partial u_{2,0}}{\partial x_1} \\ \phi_2 + \frac{\partial u_{3,0}}{\partial x_1} \\ \frac{\partial \phi_3}{\partial x_1} \\ \frac{\partial \phi_2}{\partial x_1} \\ \frac{\partial \phi_1}{\partial x_1} \end{bmatrix} \tag{32}$$

From Eqs. (30–32), we get six linear algebraic equations that can be written in the matrix form:

$$[f(\omega)]\{d_j\} = 0 \tag{33}$$

For a nontrivial solution, it is required that

$$|f(\omega)| = 0 \tag{34}$$

A solution to Eq. (34) results in the natural frequencies of the structure.

III. Frequencies and Wavelengths

It is interesting to plot the frequencies with respect to the wavelengths of the coordinates of vibration of interest. Because the torsional, bending, and longitudinal waves travel at different speeds, the wavelengths for these coordinates will be different for the same frequency. The equivalent beam model for this structure provides a simple tool to find the wave speeds of different coordinates [3]. For example, the bending-wave speed, a dispersive wave, is given by

$$c = \sqrt[4]{\frac{A_L E_L L_b^2 L_L}{6(A_b L_b \rho_b + A_d L_d \rho_d + A_L L_L \rho_L)}}\sqrt{2\pi f} \tag{35}$$

For the longitudinal-wave speed, we get

$$c = \sqrt{\frac{A_L E_L L_L}{(A_b L_b \rho_b + A_d L_d \rho_d + A_L L_L \rho_L)}} \tag{36}$$

and the relation for the torsional-wave speed can be written as

$$c = \sqrt{\frac{A_d A_L E_d E_L L_b^2 L_d L_L^2}{2(A_b L_b \rho_b + A_d L_d \rho_d + 2A_L L_L \rho_L)(A_d E_d L_d L_L^3 + A_L E_L L_d^4)}} \tag{37}$$

Finally, using the preceding and the relation for the wavelengths, which is given by $\lambda = c/f$, the wavelengths of the frequencies of different coordinates of vibrations can be found.

IV. Numerical Results

In the presented approach, an equivalent beamlike continuum model is found for this structure and, subsequently, the governing partial differential equations of motion are found. A finite element model was developed in MATLAB to validate the accuracy of the natural frequencies of the continuum model.

A comparison of the natural frequencies for the Timoshenko, Euler–Bernoulli, and the FEA is presented in Tables 2–5, for free–free boundary conditions. The first natural frequency is a repeated frequency of zero value (rigid-body motion), associated with the three coordinates of vibration in each set of the coupled PDE. The results show that the natural frequencies of the Timoshenko model have better accuracy relative to the Euler–Bernoulli model. The average error of the Timoshenko model for the $U_{3,0}$, $U_{1,0}$, and Φ_2 coordinates is 0.64% for the point-mass model and 0.51% for the solid-panel model. These values are 1.64 and 1.51% for the $U_{2,0}$, Φ_1, and Φ_3 coordinates, respectively. The highest error of Euler–Bernoulli for both kinetic energy models is 46% for the $U_{3,0}$, $U_{1,0}$, and Φ_2 coordinates and 15% for the $U_{2,0}$, Φ_1, and Φ_3 coordinates, whereas this value is 2.8% for the Timoshenko model for both sets of coordinates.

Table 2 Natural frequencies of the point-mass model for bending, longitudinal, and rotation of the cross section ($U_{3,0}$, $U_{1,0}$, and Φ_2) in rad/s

FEA	Timoshenko	Error %	Euler–Ber.	Error %
0	0	0	0	0
0.4633	0.4604	0.6259	0.4621	0.2590
1.2646	1.2567	0.6247	1.2737	0.7196
2.4425	2.4272	0.6264	2.4970	2.2313
3.9587	3.9343	0.6164	4.1277	4.2691
5.7737	5.7380	0.6183	6.1661	6.7963
7.8445	7.7974	0.6004	8.6122	9.7865
10.1287	10.0687	0.5924	11.4659	13.2021
12.5860	12.5165	0.5522	14.7274	17.0141
15.1802	15.0895	0.5975	18.3965	21.1875
16.3500	15.8940	2.7890	15.8933	2.7933
17.8796	17.7986	0.4530	22.4733	25.6924
20.6570	20.5828	0.3592	26.9577	30.5015
23.4899	23.4209	0.2937	31.8498	35.5893
26.3596	26.3152	0.1684	37.1497	40.9342
29.2511	29.2238	0.0933	42.8572	46.5148

Table 3 Natural frequencies of the solid-panel model for bending, longitudinal, and rotation of the cross section ($U_{3,0}$, $U_{1,0}$, and Φ_2) in rad/s

FEA	Timoshenko	Error %	Euler–Ber.	Error %
0	0	0	0	0
0.4634	0.4600	0.7337	0.4621	0.2590
1.2644	1.2547	0.7672	1.2737	0.7196
2.4406	2.4210	0.8031	2.4970	2.2313
3.9524	3.9200	0.8198	4.1277	4.2691
5.7587	5.7110	0.8283	6.1661	6.7963
7.8149	7.7530	0.7921	8.6122	9.7865
10.0768	10.0026	0.7363	11.4659	13.2021
12.5026	12.4254	0.6175	14.7274	17.0141
15.0541	14.9729	0.5394	18.3965	21.1875
16.3540	15.8919	2.8256	15.8933	2.7933
17.6976	17.6515	0.2605	22.4733	25.6924
20.4036	20.4072	−0.0176	26.9577	30.5015
23.1472	23.2172	−0.3024	31.8498	35.5893
25.9071	26.0849	−0.6863	37.1497	40.9342
28.6657	28.9695	−1.0598	42.8572	46.5148

Table 4 Natural frequencies of the point-mass model for bending, torsional, and rotation of the cross section ($U_{2,0}$, Φ_1, and Φ_2) in rad/s

FEA	Timoshenko	Error %	Euler–Ber.	Error %
0	0	0	0	0
0.4628	0.4595	0.7131	0.4614	0.3025
1.2572	1.2480	0.7318	1.2657	0.6761
2.1883	2.1267	2.8150	2.1269	2.8058
2.4111	2.3926	0.7673	2.4623	2.1235
3.8714	3.8396	0.8214	4.0239	3.9391
4.3839	4.2617	2.7875	4.2638	2.7396
5.5834	5.5334	0.8955	5.9151	5.9408
6.5920	6.4124	2.7245	6.4245	2.5410
7.4924	7.4172	1.0037	8.0795	7.8359
8.8151	8.5858	2.6012	8.6303	2.0964
9.5497	9.4388	1.1613	10.4355	9.2757
11.0531	10.7878	2.4002	10.9103	1.2919
11.7173	11.5557	1.3792	12.8912	10.0185
13.2972	13.0155	2.1185	13.2978	0.0045
13.9759	13.7456	1.6478	15.3719	9.9886

Table 5 Natural frequencies of the solid-panel model for bending, torsion, and rotation of the cross section ($U_{2,0}$, Φ_1, and Φ_3) in rad/s

FEA	Timoshenko	Error %	Euler–Ber.	Error %
0	0	0	0	0
0.4630	0.4593	0.7991	0.4614	0.3456
1.2583	1.2475	0.8583	1.2662	0.6278
2.4144	2.3920	0.9278	2.4650	2.0958
3.4073	3.3119	2.7999	3.3128	2.7735
3.8827	3.8440	0.9967	4.0374	3.9843
5.5954	5.5365	1.0527	5.9380	6.1229
6.8379	6.6498	2.7508	6.6615	2.5797
7.5165	7.4361	1.0696	8.1637	8.6104
9.5880	9.4865	1.0586	10.0349	4.6610
10.2790	10.0035	2.6802	10.6558	3.6657
11.7728	11.6534	1.0142	13.3713	13.5779
13.6530	13.3401	2.2918	13.4713	1.3308
14.1314	13.9593	1.2179	16.2639	15.0905
16.2021	16.0510	0.9326	16.9874	4.8469
17.3992	16.9964	2.3150	19.2925	10.8815

In the Euler–Bernoulli model, the equations of motion for bending in the x_3 direction and for the longitudinal vibrations remain the same for both kinetic energy models. This is because the difference between the kinetic energy expressions in these two models is related to the rotary inertia terms Φ_2, Φ_3, and because they do not appear in the Euler–Bernoulli model, the equations are identical.

It is also interesting to examine the frequencies of the continuum model and the FEA versus wavelengths. These results are shown in Figs. 6–11. As shown, the wavelengths for the longitudinal modes

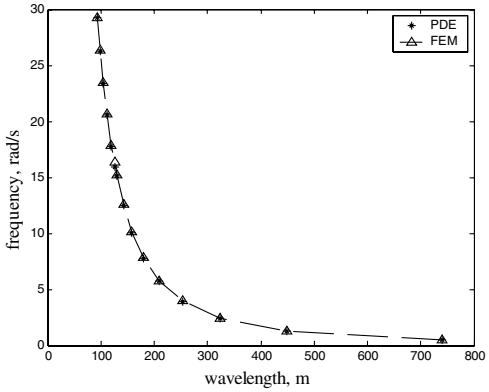

Fig. 6 Bending natural frequencies $U_{3,0}$ for the point-mass model.

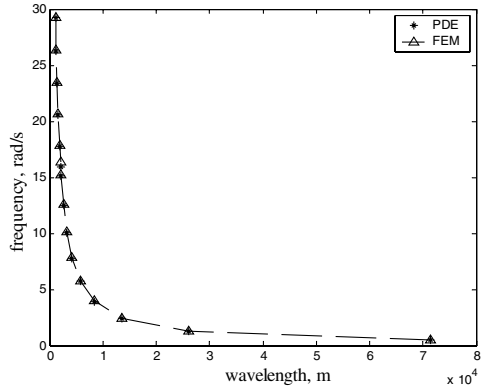

Fig. 7 Longitudinal natural frequencies for the point-mass model.

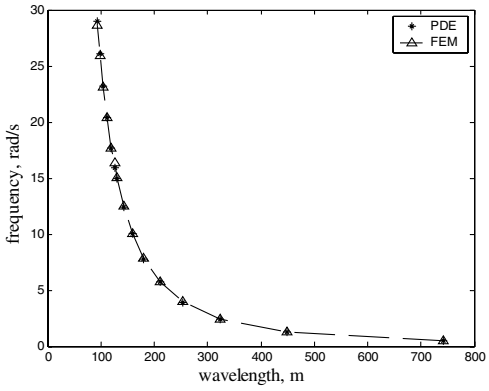

Fig. 8 Bending natural frequencies $U_{3,0}$ for the solid-panel model.

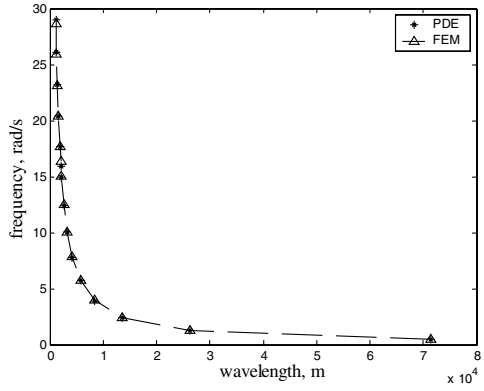

Fig. 9 Longitudinal natural frequencies for the solid-panel model.

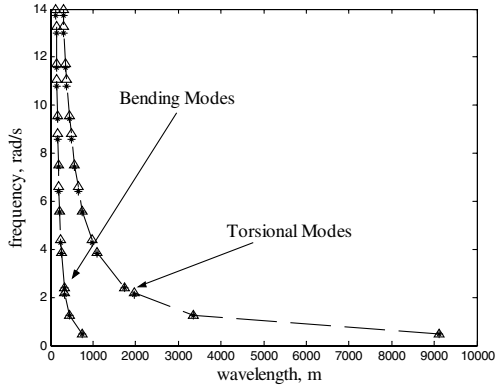

Fig. 10 Natural frequencies of bending, torsional and cross-sectional rotation ($U_{2,0}$, Φ_1, and Φ_3) for the point-mass model.

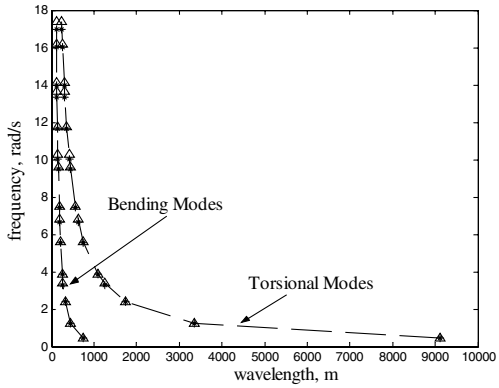

Fig. 11 Natural frequencies of bending, torsional and cross-sectional rotation ($U_{2,0}$, Φ_1, and Φ_3) for the solid-panel model.

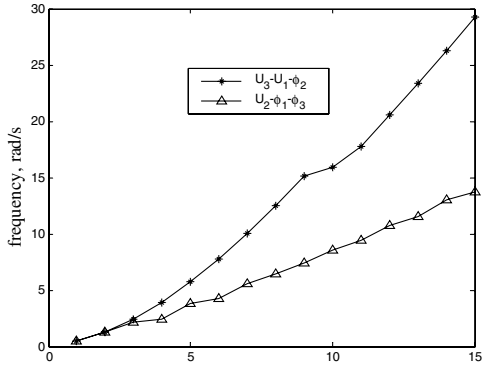

Fig. 12 Natural frequencies of the point-mass model for $U_{2,0}$, Φ_1, and Φ_3 and $U_{3,0}$, $U_{1,0}$, and Φ_2.

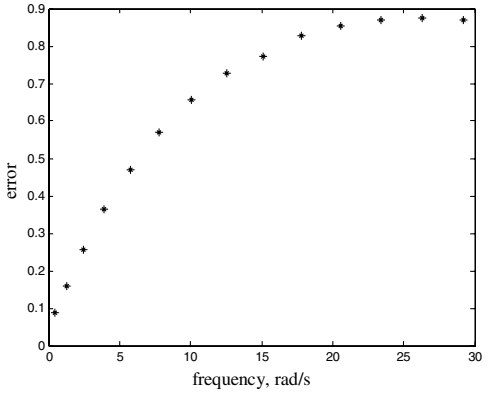

Fig. 13 Difference percentage of natural frequencies of the point mass and solid-panel models for $U_{3,0}$, $U_{1,0}$, and Φ_2.

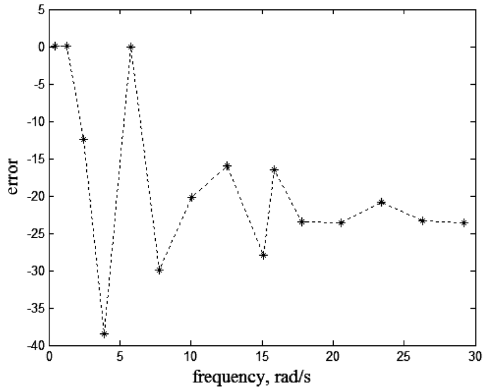

Fig. 14 Difference percentage of natural frequencies of the point mass and solid models for $U_{2,0}$, Φ_1, and Φ_3.

are higher for the same values of frequencies when compared with the bending modes. This is because the longitudinal waves travel at higher speeds and thus have higher wavelengths. A similar observation can be made for the torsional modes when compared with the bending coordinates (Figs. 10 and 11).

In Fig. 12, the natural frequencies of the Timoshenko point-mass model are compared for the $U_{3,0}$, $U_{1,0}$, and Φ_2 and $U_{2,0}$, Φ_1, and Φ_3 coordinates. It is observed that the fundamental natural frequencies are very close for these two sets of coordinates, whereas the difference grows for higher modes. The symmetry of the structure is lost due to the added panel, which causes the deviation between the frequencies of the bending coordinates in different directions; this effect is more prominent at higher modes.

Frequency estimations from the two kinetic energy models are compared in Figs. 13 and 14. It is observed that this difference between the two kinetic energy models is smaller for the $U_{3,0}$, $U_{1,0}$, and Φ_2 coordinates and has an exponential pattern. This is because in the point-mass model, the mass of the panel is concentrated at the edge of the truss; therefore, the main modes that are accounted for differently in this model are the torsional modes, which results in a bigger difference of the frequencies, mainly for the $U_{2,0}$, Φ_1, and Φ_3 coordinates. For the first few modes, the accuracy of the point-mass model is sufficient for both sets of coupled coordinates. The model shows less accuracy for the higher modes.

V. Conclusions

A continuum-modeling approach is presented for a structure that consists of repeated lattice elements supporting a radar panel. The governing partial differential equations of motion are derived for both the truss-panel assembly and the original truss with no panel. Two kinetic energy models are suggested to account for the radar mass in the continuum models. In the first, the mass of the panel is distributed among the bottom joints, and in the other, each segment of the panel is modeled as a solid plate with a constant density. In both models, the strain energy of the panel is ignored. Finally, two continuum-beam models are derived for the structure under study: Timoshenko and Euler–Bernoulli. The equations for the Timoshenko model of the truss-panel assembly along the six coordinates of vibration decouple into two sets of PDEs, each containing three coordinates of vibration. One of the bending coordinates is coupled with the longitudinal vibration and the rotation of cross section, which forms an equation similar to an extended Timoshenko beam theory. Similarly, the torsional coordinate is coupled with the other bending and rotational coordinates of the cross section. This is in contrast to the original truss, in which the two bending coordinates decouple from the longitudinal and the torsional vibrations. A simpler continuum model for the structure is derived using the assumptions of an Euler–Bernoulli beam; that is, by ignoring the shear strain in the potential energy and the rotary inertia effects in the kinetic energy expressions. In this model, one of the bending coordinates (perpendicular to the panel) is decoupled from other coordinates and has a form similar to the bending of an Euler–Bernoulli beam; it is shown that this bending

equation is similar for both kinetic energy models. It is also shown that for the first few modes, the point-mass model accuracy is enough for the estimation of natural frequencies. The results for these models are compared with a standard FEA of the structure for the purpose of validation. It is shown that the Timoshenko continuum model compares well with the FEA method. The proposed PDE model can be used to apply existing methods for control design of distributed parameter systems. The equations of motion for the case of the truss with no panel are also derived and presented in this work. It is shown that the bending equations of this structure are similar to those of a conventional Timoshenko beam. The torsional and longitudinal equations of motion for the truss (no panel) decouple from other coordinates and they have a form similar to the equations of a bar element.

Appendix A: Strain Energy

In this section, some of the previously made assumptions by Noor [7] are used to find the strain energy expressions for a repeating element of the structure shown in Fig. A1. Using the displacement relations in Eq. (1) and its derivatives, the strain components for each of the bar members can be found in terms of the strain components evaluated at the center of the element. Using a Taylor series expansion, these expressions can be expanded around the center of the midcross section of the element and along the x_1 coordinate. Finally, the strain energy of the repeating element, which consists of the 18 bar members, are found in terms of the total of 21 strain and curvature components and their derivatives.

To find the equivalent continuum model, the assumptions of the local free deformation should hold [7]. This means that forces associated with the local deformations should vanish, and therefore the derivatives of the strain energy with respect to the following strain gradients should be zero, so that we have

$$\frac{\partial U_{\text{total}}}{\partial(\partial\varepsilon_{1,0}/\partial x_1)}=0\Rightarrow 6\Big[A_dE_dL_dL_L^3+A_LE_L\Big(L_b^2+L_L^2\Big)^2\Big]\frac{\partial\varepsilon_{1,0}}{\partial x_1}+A_dE_dL_b^2L_dL_L\Big(3\frac{\partial\varepsilon_{2,0}}{\partial x_1}+3\frac{\partial\varepsilon_{3,0}}{\partial x_1}-2\sqrt{3}\kappa_{t,0}\Big)=0 \tag{A1a}$$

$$\frac{\partial U_{\text{total}}}{\partial(\partial\kappa_{2,0}/\partial x_1)}=0\Rightarrow -A_dE_dL_bL_dL_L\frac{\partial\varepsilon_{2,0}}{\partial x_1}+A_dE_dL_bL_dL_L\frac{\partial\varepsilon_{3,0}}{\partial x_1}+4A_LE_L\Big(L_b^2+L_L^2\Big)^2\frac{\partial\kappa_{2,0}}{\partial x_1}+A_dE_dL_dL_L\Big[L_L^2\frac{\partial\kappa_{2,0}}{\partial x_1}+2\sqrt{3}\Big(L_b\frac{\partial\varepsilon_{23,0}}{\partial x_1}+4\varepsilon_{13,0}\Big)\Big]=0 \tag{A1b}$$

$$\frac{\partial U_{\text{total}}}{\partial(\partial\kappa_{3,0}/\partial x_1)}=0\Rightarrow 4A_LE_L\Big(L_b^2+L_L^2\Big)^2\frac{\partial\kappa_{3,0}}{\partial x_1}+A_dE_dL_dL_L\Big(-\sqrt{3}L_b\frac{\partial\varepsilon_{2,0}}{\partial x_1}+\sqrt{3}L_b\frac{\partial\varepsilon_{3,0}}{\partial x_1}-2L_b\frac{\partial\varepsilon_{23,0}}{\partial x_1}+L_L^2\frac{\partial\kappa_{3,0}}{\partial x_1}+8\sqrt{3}\varepsilon_{12,0}\Big)=0 \tag{A1c}$$

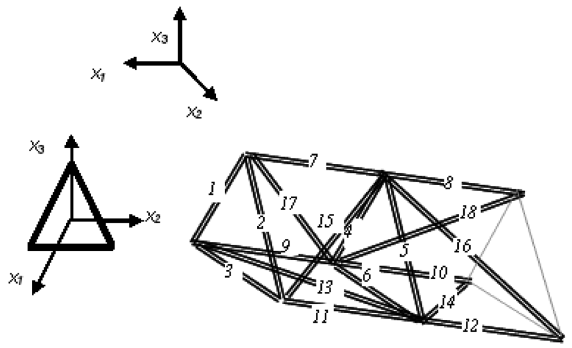

Fig. A1 Bar members in an element and reference coordinate system attached to the midcross section.

$$\frac{\partial U_{\text{total}}}{\partial(\partial\varepsilon_{12,0}/\partial x_1)}=0\Rightarrow 3L_bL_L^2\frac{\partial^2\varepsilon_{2,0}}{\partial x_1^2}-3L_bL_L^2\frac{\partial^2\varepsilon_{3,0}}{\partial x_1^2}+4L_b\Big(\sqrt{3}L_L^2\frac{\partial^2\varepsilon_{23,0}}{\partial x_1^2}+6\varepsilon_{2,0}-6\varepsilon_{3,0}\Big)-8L_L^2\Big(6\frac{\partial\varepsilon_{12,0}}{\partial x_1}+\sqrt{3}\kappa_{3,0}\Big)=0 \tag{A1d}$$

$$\frac{\partial U_{\text{total}}}{\partial(\partial\varepsilon_{13,0}/\partial x_1)}=0\Rightarrow \sqrt{3}L_bL_L^2\frac{\partial^2\varepsilon_{2,0}}{\partial x_1^2}-24L_b\varepsilon_{23,0}-L_L^2\Big(\sqrt{3}L_b\frac{\partial^2\varepsilon_{3,0}}{\partial x_1^2}+3L_b\frac{\partial^2\varepsilon_{23,0}}{\partial x_1^2}+24\frac{\partial\varepsilon_{13,0}}{\partial x_1}+4\sqrt{3}\kappa_{2,0}\Big)=0 \tag{A1e}$$

$$\frac{\partial U_{\text{total}}}{\partial(\partial\kappa_{t,0}/\partial x_1)}=0\Rightarrow L_L^2\Big[L_b^2\Big(\sqrt{3}\frac{\partial^2\varepsilon_{2,0}}{\partial x_1^2}+\sqrt{3}\frac{\partial^2\varepsilon_{3,0}}{\partial x_1^2}-4\frac{\partial\kappa_{t,0}}{\partial x_1}\Big)+16\sqrt{3}\varepsilon_{1,0}\Big]+8\sqrt{3}L_b^2(\varepsilon_{2,0}+\varepsilon_{3,0})=0 \tag{A1f}$$

$$\begin{aligned}\frac{\partial U_{\text{total}}}{\partial(\partial^2\varepsilon_{2,0}/\partial x_1^2)}=0\Rightarrow{}&L_L^2\Big[13A_dE_dL_b^3L_d+72A_bE_b\Big(L_b^2+L_L^2\Big)^2\Big]\frac{\partial^2\varepsilon_{2,0}}{\partial x_1^2}\\&+L_L^2\Big[-A_dE_dL_b^3L_d+24A_bE_b\Big(L_b^2+L_L^2\Big)^2\Big]\frac{\partial^2\varepsilon_{3,0}}{\partial x_1^2}\\&+8\Big[6A_bE_bL_L\Big(L_b^2+L_L^2\Big)^2\Big(3\frac{\partial\varepsilon_{2,0}}{\partial x_1}+\frac{\partial\varepsilon_{3,0}}{\partial x_1}\Big)\\&-A_dE_dL_b^2L_dL_L^2\Big(6\frac{\partial\varepsilon_{12,0}}{\partial x_1}+4\sqrt{3}\frac{\partial\varepsilon_{13,0}}{\partial x_1}\Big)-\sqrt{3}A_dE_dL_b^3L_dL_L^2\frac{\partial\kappa_{t,0}}{\partial x_1}\\&+12A_dE_dL_bL_dL_L^2\varepsilon_{1,0}+18A_bE_b\Big(L_b^4+L_L^4\Big)\varepsilon_{2,0}\\&+6A_bE_b\Big(L_b^4+L_L^4\Big)\varepsilon_{3,0}+12A_bE_bL_b^2L_L^2(3\varepsilon_{2,0}+\varepsilon_{3,0})\\&+A_dE_dL_b^3L_d(9\varepsilon_{2,0}+3\varepsilon_{3,0}-4\sqrt{3}\varepsilon_{23,0})\\&-A_dE_dL_b^2L_dL_L^2(2\kappa_{2,0}+\sqrt{3}\kappa_{3,0})\Big]=0\end{aligned} \tag{A1g}$$

$$\begin{aligned}\frac{\partial U_{\text{total}}}{\partial(\partial^2\varepsilon_{3,0}/\partial x_1^2)}=0\Rightarrow{}&L_L^2\Big[-A_dE_dL_b^3L_d+24A_bE_b\Big(L_b^2+L_L^2\Big)^2\Big]\\&\times\frac{\partial^2\varepsilon_{2,0}}{\partial x_1^2}+L_L^2\Big[13A_dE_dL_b^3L_d+72A_bE_b\Big(L_b^2+L_L^2\Big)^2\Big]\frac{\partial^2\varepsilon_{3,0}}{\partial x_1^2}\\&+8\Big[6A_bE_bL_L\Big(L_b^2+L_L^2\Big)^2\Big(\frac{\partial\varepsilon_{2,0}}{\partial x_1}+3\frac{\partial\varepsilon_{3,0}}{\partial x_1}\Big)\\&+6A_bE_b\Big(L_b^4+L_L^4\Big)\varepsilon_{2,0}+12A_bE_bL_b^2L_L^2(\varepsilon_{2,0}+3\varepsilon_{3,0})\\&+18A_bE_b\Big(L_b^4+L_L^4\Big)\varepsilon_{3,0}+A_dE_dL_b^2L_dL_L^2\Big(6\frac{\partial\varepsilon_{12,0}}{\partial x_1}\\&+4\sqrt{3}\frac{\partial\varepsilon_{13,0}}{\partial x_1}+2\kappa_{2,0}+\sqrt{3}\kappa_{3,0}\Big)-\sqrt{3}A_dE_dL_b^3L_dL_L^2\frac{\partial\kappa_{t,0}}{\partial x_1}\\&+12A_dE_dL_bL_dL_L^2\varepsilon_{1,0}+A_dE_dL_b^3L_d(3\varepsilon_{2,0}+9\varepsilon_{3,0}\\&+4\sqrt{3}\varepsilon_{23,0})\Big]=0\end{aligned} \tag{A1h}$$

$$\frac{\partial U_{\text{total}}}{\partial(\partial^2\varepsilon_{23,0}/\partial x_1^2)} = 0 \Rightarrow L_L^2[7A_dE_dL_b^3L_d + 24A_bE_b(L_b^2+L_L^2)^2] \times \frac{\partial^2\varepsilon_{23,0}}{\partial x_1^2} + 48A_bE_b(L_b^2+L_L^2)^2\left(L_L\frac{\partial\varepsilon_{23,0}}{\partial x_1}+\varepsilon_{23,0}\right) + 4A_dE_dL_b^2L_d\left[2L_b(\sqrt{3}\varepsilon_{2,0}-\sqrt{3}\varepsilon_{3,0}+3\varepsilon_{23,0}) + L_L^2\left(-4\sqrt{3}\frac{\partial\varepsilon_{12,0}}{\partial x_1}+6\frac{\partial\varepsilon_{13,0}}{\partial x_1}+\sqrt{3}\kappa_{2,0}-2\kappa_{3,0}\right)\right]=0 \quad \text{(A1i)}$$

Similarly, to get a shear deformation type of beam, the extensional stresses along the x_2 and x_3 directions and the shear stress in 23 directions should vanish, because these do not exist in a beam model. Therefore, the following should hold

$$\frac{\partial U_{\text{total}}}{\partial\varepsilon_{2,0}} = 0 \Rightarrow [A_dE_dL_b^3L_d + 2A_bE_b(L_b^2+L_L^2)^2] \times\left(\frac{\partial^2\varepsilon_{2,0}}{\partial x_1^2}+\frac{\partial^2\varepsilon_{3,0}}{\partial x_1^2}\right)+12A_bE_b(L_b^2+L_L^2)^2 \times\left(3L_L\frac{\partial\varepsilon_{2,0}}{\partial x_1}+L_L\frac{\partial\varepsilon_{3,0}}{\partial x_1}+6\varepsilon_{2,0}+2\varepsilon_{3,0}\right) + 4A_dE_dL_bL_d\left[24L_L^2\varepsilon_{1,0}+L_b^2\left[\sqrt{3}L_L^2\left(\frac{\partial^2\varepsilon_{23,0}}{\partial x_1^2}-2\frac{\partial\kappa_{t,0}}{\partial x_1}\right)+6(3\varepsilon_{2,0}+\varepsilon_{3,0})\right]-2L_bL_L^2\left(6\frac{\partial\varepsilon_{12,0}}{\partial x_1}+\sqrt{3}\kappa_{3,0}\right)\right]=0$$

$$\frac{\partial U_{\text{total}}}{\partial\varepsilon_{3,0}} = 0 \Rightarrow [A_dE_dL_b^3L_d + 2A_bE_b(L_b^2+L_L^2)^2] \times\left(3L_L^2\frac{\partial^2\varepsilon_{2,0}}{\partial x_1^2}+9L_L^2\frac{\partial^2\varepsilon_{3,0}}{\partial x_1^2}\right)+12A_bE_b(L_b^2+L_L^2)^2 \times\left(L_L\frac{\partial\varepsilon_{2,0}}{\partial x_1}+3L_L\frac{\partial\varepsilon_{3,0}}{\partial x_1}+2\varepsilon_{2,0}+6\varepsilon_{3,0}\right) - 4A_dE_dL_bL_d\left[-24L_L^2\varepsilon_{1,0}+L_b^2\left[\sqrt{3}L_L^2\left(\frac{\partial^2\varepsilon_{23,0}}{\partial x_1^2}+2\frac{\partial\kappa_{t,0}}{\partial x_1}\right)-6(\varepsilon_{2,0}+3\varepsilon_{3,0})\right]-2L_bL_L^2\left(6\frac{\partial\varepsilon_{12,0}}{\partial x_1}+\sqrt{3}\kappa_{3,0}\right)\right]=0$$

$$\frac{\partial U_{\text{total}}}{\partial\varepsilon_{23,0}} = 0 \Rightarrow 6A_bE_bL_b(L_b^2+L_L^2)^2\left(L_L^2\frac{\partial^2\varepsilon_{23,0}}{\partial x_1^2}+2L_L\frac{\partial\varepsilon_{23,0}}{\partial x_1}+4\varepsilon_{23,0}\right)-A_dE_dL_b^3L_d\left[\sqrt{3}L_bL_L^2\frac{\partial^2\varepsilon_{2,0}}{\partial x_1^2}-24L_b\varepsilon_{23,0} -L_L^2\left(\sqrt{3}L_b\frac{\partial^2\varepsilon_{3,0}}{\partial x_1^2}+3L_b\frac{\partial^2\varepsilon_{23,0}}{\partial x_1^2}+24\frac{\partial\varepsilon_{13,0}}{\partial x_1}+4\sqrt{3}\kappa_{2,0}\right)\right] =0 \quad \text{(A2)}$$

On the other hand, the compatibility condition requires that the strain components at the plane of the cross section of the adjacent elements be the same, or [7]

$$\frac{\partial\varepsilon_{2,0}}{\partial x_1}=0, \qquad \frac{\partial\varepsilon_{3,0}}{\partial x_1}=0, \qquad \frac{\partial\varepsilon_{23,0}}{\partial x_1}=0 \quad \text{(A3)}$$

Equations (A1–A3) provide us with a total of 15 equations to solve for the 15 strain components and their gradients of the original 21 unknowns stated before. This results in six independent strain and curvature components. The solution for the other strains can be found as follows:

$$\frac{\partial\varepsilon_{12,0}}{\partial x_1}=-\frac{\kappa_{3,0}}{2\sqrt{3}}, \qquad \frac{\partial\kappa_{t,0}}{\partial x_1}=\frac{4\sqrt{3}\varepsilon_{1,0}}{L_b^2}, \qquad \frac{\partial\varepsilon_{13,0}}{\partial x_1}=-\frac{\kappa_{2,0}}{2\sqrt{3}}$$

$$\varepsilon_{2,0}=0, \qquad \varepsilon_{3,0}=0, \qquad \varepsilon_{23,0}=0$$

$$\frac{\partial\varepsilon_{1,0}}{\partial x_1}=\frac{A_dE_dL_b^2L_dL_L\kappa_{t,0}}{\sqrt{3}\left(A_dE_dL_dL_L^3+A_LE_L\left(L_b^2+L_L^2\right)^2\right)}$$

$$\frac{\partial\kappa_{3,0}}{\partial x_1}=-\frac{8\sqrt{3}A_dE_dL_dL_L\varepsilon_{12,0}}{A_dE_dL_dL_L^3+4A_LE_L\left(L_b^2+L_L^2\right)^2}$$

$$\frac{\partial\kappa_{2,0}}{\partial x_1}=-\frac{8\sqrt{3}A_dE_dL_dL_L\varepsilon_{13,0}}{A_dE_dL_dL_L^3+4A_LE_L\left(L_b^2+L_L^2\right)^2}, \qquad \frac{\partial^2\varepsilon_{2,0}}{\partial x_1^2}=0$$

$$\frac{\partial^2\varepsilon_{23,0}}{\partial x_1^2}=0, \qquad \frac{\partial^2\varepsilon_{3,0}}{\partial x_1^2}=0 \quad \text{(A4)}$$

Using the solutions found in Eq. (A4), the strain energy of a repeating element can be found in terms of the strain and curvature components $\varepsilon_{1,0}$, $\kappa_{2,0}$, $\kappa_{3,0}$, $\kappa_{t,0}$, $\varepsilon_{12,0}$, and $\varepsilon_{13,0}$ as follows:

$$U = 3A_LE_LL_L(\varepsilon_{1,0})^2+\frac{1}{2}A_LE_LL_b^2L_L[(\kappa_{2,0})^2+(\kappa_{3,0})^2] + \frac{24A_dA_LE_dE_LL_b^2L_dL_L^2}{A_dE_dL_dL_L^3+4A_LE_L\left(L_b^2+L_L^2\right)^2}[(\varepsilon_{12,0})^2+(\varepsilon_{13,0})^2] + \frac{A_dA_LE_dE_LL_b^4L_dL_L^2}{4\left[A_dE_dL_dL_L^3+A_LE_L\left(L_b^2+L_L^2\right)^2\right]}(\kappa_{t,0})^2 \quad \text{(A5)}$$

The following can be easily found:

$$\varepsilon_{1,0}=\frac{\partial u_{1,0}}{\partial x_1}, \qquad \varepsilon_{12,0}=\frac{1}{2}\left(\frac{\partial u_{2,0}}{\partial x_1}-\phi_3\right)$$

$$\varepsilon_{13,0}=\frac{1}{2}\left(\frac{\partial u_{3,0}}{\partial x_1}+\phi_2\right), \qquad \kappa_{2,0}=\frac{\partial\phi_3}{\partial x_1}, \qquad \kappa_{3,0}=\frac{\partial\phi_2}{\partial x_1} \quad \text{(A6)}$$

$$\kappa_{t,0}=\frac{\partial\phi_1}{\partial x_1}$$

Equations (A5) and (A6) result in

$$U = 3A_LE_LL_L\left(\frac{\partial u_{1,0}}{\partial x_1}\right)^2+\frac{1}{2}A_LE_LL_b^2L_L\left[\left(\frac{\partial\phi_3}{\partial x_1}\right)^2+\left(\frac{\partial\phi_2}{\partial x_1}\right)^2\right] + \frac{24A_dA_LE_dE_LL_b^2L_dL_L^2}{A_dE_dL_dL_L^3+4A_LE_L\left(L_b^2+L_L^2\right)^2}\left(\left[\frac{1}{2}\left(\frac{\partial u_{2,0}}{\partial x_1}-\phi_3\right)\right]^2 + \left[\frac{1}{2}\left(\frac{\partial u_{3,0}}{\partial x_1}+\phi_2\right)\right]^2\right) + \frac{A_dA_LE_dE_LL_b^4L_dL_L^2}{4\left[A_dE_dL_dL_L^3+A_LE_L\left(L_b^2+L_L^2\right)^2\right]}\left(\frac{\partial\phi_1}{\partial x_1}\right)^2 \quad \text{(A7)}$$

Appendix B: Kinetic Energy

It can be shown that the kinetic energy of a bar element can be written in the following form:

$$T=\tfrac{1}{6}\rho Al\left(V_{1x}^2+V_{1y}^2+V_{1z}^2+V_{2x}^2+V_{2y}^2+V_{2z}^2+V_{1x}V_{2x} + V_{1y}V_{2y}+V_{1z}V_{2z}\right) \quad \text{(B1)}$$

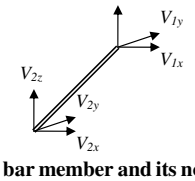

Fig. B1 Schematic of a bar member and its nodal velocity components.

where subscripts x, y, and z show different velocity components, and subscripts 1 and 2 refer to each of the two ends of the bar, as shown in Fig. B1.

Using Eq. (1), the kinetic energy of the bar member k of the repeating truss element shown in Fig. A1 can be found as follows:

$$\begin{aligned}T_k = {} & \frac{1}{6}\rho_k A_k L_k\left[\left(\frac{\partial u_{1,0}}{\partial t} - x_{2,1,k}\frac{\partial \phi_3}{\partial t} + x_{3,1,k}\frac{\partial \phi_2}{\partial t}\right)^2\right. \\ & + \left(\frac{\partial u_{2,0}}{\partial t} - x_{3,1,k}\frac{\partial \phi_1}{\partial t}\right)^2 + \left(\frac{\partial u_{1,0}}{\partial t} - x_{2,1,k}\frac{\partial \phi_3}{\partial t} + x_{3,1,k}\frac{\partial \phi_2}{\partial t}\right) \\ & \times \left(\frac{\partial u_{1,0}}{\partial t} - x_{2,2,k}\frac{\partial \phi_3}{\partial t} + x_{3,2,k}\frac{\partial \phi_2}{\partial t}\right) + \left(\frac{\partial u_{3,0}}{\partial t} + x_{2,1,k}\frac{\partial \phi_1}{\partial t}\right)^2 \\ & + \left(\frac{\partial u_{1,0}}{\partial t} - x_{2,2,k}\frac{\partial \phi_3}{\partial t} + x_{3,2,k}\frac{\partial \phi_2}{\partial t}\right)^2 + \left(\frac{\partial u_{2,0}}{\partial t} - x_{3,2,k}\frac{\partial \phi_1}{\partial t}\right)^2 \\ & + \left(\frac{\partial u_{3,0}}{\partial t} + x_{2,2,k}\frac{\partial \phi_1}{\partial t}\right)^2 + \left(\frac{\partial u_{2,0}}{\partial t} - x_{3,1,k}\frac{\partial \phi_1}{\partial t}\right) \\ & \times \left(\frac{\partial u_{2,0}}{\partial t} - x_{3,2,k}\frac{\partial \phi_1}{\partial t}\right) + \left(\frac{\partial u_{3,0}}{\partial t} + x_{2,1,k}\frac{\partial \phi_1}{\partial t}\right) \\ & \times \left.\left(\frac{\partial u_{3,0}}{\partial t} + x_{2,2,k}\frac{\partial \phi_1}{\partial t}\right)\right] \end{aligned} \tag{B2}$$

The kinetic energy of the truss element is the summation of those of the 18 bar members and can be found as

$$\begin{aligned}T_{\text{total}} = \sum_{k=1}^{18} T_k = {} & 3(A_b L_b \rho_b + A_d L_d \rho_d + A_L L_L \rho_L) \\ & \times \left[\left(\frac{\partial u_{1,0}}{\partial t}\right)^2 + \left(\frac{\partial u_{2,0}}{\partial t}\right)^2 + \left(\frac{\partial u_{3,0}}{\partial t}\right)^2\right] \\ & + \frac{L_b^2(A_b L_b \rho_b + A_d L_d \rho_d + 2A_L L_L \rho_L)}{4} \\ & \times \left[2\left(\frac{\partial \phi_1}{\partial t}\right)^2 + \left(\frac{\partial \phi_2}{\partial t}\right)^2 + \left(\frac{\partial \phi_3}{\partial t}\right)^2\right] \end{aligned} \tag{B3}$$

Making the assumptions of the point-mass model, the kinetic energy of the panel can be found in terms of the displacement components as follows:

$$\begin{aligned}T_p = {} & \frac{m_p}{2}\left[\left(\frac{\partial u_{1,0}}{\partial t} + \frac{L_b}{2}\frac{\partial \phi_3}{\partial t} - \frac{L_b\sqrt{3}}{6}\frac{\partial \phi_2}{\partial t}\right)^2\right. \\ & \left. + \left(\frac{\partial u_{2,0}}{\partial t} + \frac{L_b\sqrt{3}}{6}\frac{\partial \phi_1}{\partial t}\right)^2 + \left(\frac{\partial u_{3,0}}{\partial t} - \frac{L_b}{2}\frac{\partial \phi_1}{\partial t}\right)^2\right] \\ & + \frac{m_p}{2}\left[\left(\frac{\partial u_{1,0}}{\partial t} - \frac{L_b}{2}\frac{\partial \phi_3}{\partial t} - \frac{L_b\sqrt{3}}{6}\frac{\partial \phi_2}{\partial t}\right)^2\right. \\ & \left. + \left(\frac{\partial u_{2,0}}{\partial t} + \frac{L_b\sqrt{3}}{6}\frac{\partial \phi_1}{\partial t}\right)^2 + \left(\frac{\partial u_{3,0}}{\partial t} + \frac{L_b}{2}\frac{\partial \phi_1}{\partial t}\right)^2\right] \end{aligned} \tag{B4}$$

where m_p is the additional mass at each joint. The preceding expression can be further simplified in the form of

$$\begin{aligned}T_p = {} & m_p\left[\left(\frac{\partial u_{3,0}}{\partial t}\right)^2 + \left(\frac{\partial u_{1,0}}{\partial t}\right)^2 + \left(\frac{\partial u_{2,0}}{\partial t}\right)^2 + \frac{\sqrt{3}}{3}L_b\frac{\partial u_{2,0}}{\partial t}\frac{\partial \phi_1}{\partial t}\right] \\ & + m_p\left(-4\frac{\sqrt{3}}{3}L_b\frac{\partial u_{1,0}}{\partial t}\frac{\partial \phi_2}{\partial t} + \frac{L_b^2}{12}\left[4\left(\frac{\partial \phi_1}{\partial t}\right)^2 + \left(\frac{\partial \phi_2}{\partial t}\right)^2\right.\right. \\ & \left.\left. + 3\left(\frac{\partial \phi_3}{\partial t}\right)^2\right]\right) \end{aligned} \tag{B5}$$

For the plate model, the kinetic energy of the panel can be written as

$$\begin{aligned}T_p = {} & \frac{1}{2}m_{\text{panel}}\left[\left(\frac{\partial u_{1,0}}{\partial t} - \frac{L_b\sqrt{3}}{6}\frac{\partial \phi_2}{\partial t}\right)^2 + \left(\frac{\partial u_{2,0}}{\partial t} + \frac{L_b\sqrt{3}}{6}\frac{\partial \phi_1}{\partial t}\right)^2\right. \\ & \left. + \left(\frac{\partial u_{3,0}}{\partial t}\right)^2\right] + \frac{1}{2}I_1\left(\frac{\partial \phi_1}{\partial t}\right)^2 + \frac{1}{2}I_2\left(\frac{\partial \phi_2}{\partial t}\right)^2 + \frac{1}{2}I_3\left(\frac{\partial \phi_3}{\partial t}\right)^2 \end{aligned} \tag{B6}$$

where m_{panel} is the mass of the segment of the panel attached to a truss element. The preceding equation can be simplified to

$$\begin{aligned}T_p = {} & \frac{m_{\text{panel}}}{2}\left[\left(\frac{\partial u_{1,0}}{\partial t}\right)^2 + \left(\frac{\partial u_{2,0}}{\partial t}\right)^2 + \left(\frac{\partial u_{3,0}}{\partial t}\right)^2\right] + \frac{1}{2}I_1\left(\frac{\partial \phi_1}{\partial t}\right)^2 \\ & + \frac{1}{2}I_2\left(\frac{\partial \phi_2}{\partial t}\right)^2 + \frac{1}{2}I_3\left(\frac{\partial \phi_3}{\partial t}\right)^2 + \frac{L_b m_{\text{panel}}}{2\sqrt{3}}\left(\frac{\partial u_{2,0}}{\partial t}\frac{\partial \phi_1}{\partial t}\right. \\ & \left. - \frac{\partial u_{1,0}}{\partial t}\frac{\partial \phi_2}{\partial t}\right) + \frac{1}{24}L_b^2 m_{\text{panel}}\left[\left(\frac{\partial \phi_1}{\partial t}\right)^2 + \left(\frac{\partial \phi_2}{\partial t}\right)^2\right] \end{aligned} \tag{B7}$$

where the rotary inertias are

$$I_1 = \frac{m_{\text{panel}}L_b^2}{12}, \qquad I_2 = \frac{m_{\text{panel}}L_b^2}{3}, \qquad I_3 = \frac{5m_{\text{panel}}L_b^2}{12} \tag{B8}$$

Finally, the kinetic energy of the truss panel for both models can be found as

$$T = \sum_{k=1}^{18} T_k + T_p \tag{B9}$$

Appendix C: Equations of Motion

Knowing the kinetic and strain energy expressions for the truss element, Hamilton's principle can then be used to find the equations of motion for the six coordinates of vibrations ϕ_1, ϕ_2, ϕ_3, $u_{1,0}$, $u_{1,0}$, and w_0. These derivations are presented here for the point-mass model. Using Eqs. (A7), (B3), and (B5) and the variational principle, we get

$$\begin{aligned}\int_{t_1}^{t_2}\int_0^{L_{\text{tot}}}(\delta T - \delta U)\,\mathrm{d}x_1\,\mathrm{d}t = {} & \int_{t_1}^{t_2}\int_0^{L_{\text{tot}}}\left[-12L_L\left(\frac{L_b^2(A_b L_b \rho_b + A_d L_d \rho_d + 2A_L L_L \rho_L)}{4L_L}\frac{\partial^2 \phi_1}{\partial t^2}\right.\right. \\ & \left. - c_6\frac{\partial^2 \phi_1}{\partial x_1^2}\right)\delta\phi_1 - 12\left([3(A_L L_L \rho_L + A_b L_b \rho_b + A_d L_d \rho_d) + m_p]\right. \\ & \left.\times\frac{\partial^2 u_{1,0}}{\partial t^2} - c_1 L_L\frac{\partial^2 u_{1,0}}{\partial x_1^2}\right)\delta u_{1,0} - \left[12c_5 L_L \phi_2 + 12c_5 L_L\frac{\partial u_{3,0}}{\partial x_1}\right. \\ & \left. + 3L_b^2(A_b L_b \rho_b + A_d L_d \rho_d + 2A_L L_L \rho_L)\frac{\partial^2 \phi_2}{\partial t^2}\right]\delta\phi_2 \\ & - \left(L_b^2 m_p\frac{\partial^2 \phi_2}{\partial t^2} - 12c_3 L_L\frac{\partial^2 \phi_2}{\partial x_1^2} - 2\sqrt{3}L_b m_p\frac{\partial^2 u_{1,0}}{\partial t^2}\right)\delta\phi_2 \\ & - 3\left[4c_4 L_L \phi_3 + \left[L_b^2(A_b L_b \rho_b + A_d L_d \rho_d + 2A_L L_L \rho_L)\right.\right. \\ & \left.\left. + L_b^2 m_p\right]\frac{\partial^2 \phi_3}{\partial t^2} - 4L_L\left(c_2\frac{\partial^2 \phi_3}{\partial x_1^2} + c_4\frac{\partial u_{2,0}}{\partial x_1}\right)\right]\delta\phi_3 \\ & - 4L_b^2 m_p\frac{\partial^2 \phi_1}{\partial t^2}\delta\phi_1 - 12\left[[3(A_L L_L \rho_L + A_b L_b \rho_b + A_d L_d \rho_d)\right. \\ & \left. + m_p]\frac{\partial^2 u_{3,0}}{\partial t^2} - c_5 L_L\left(\frac{\partial^2 u_{3,0}}{\partial x_1^2} + \frac{\partial \phi_2}{\partial x_1}\right)\right]\delta u_{3,0} \\ & - 12\left(c_4 L_L\frac{\partial \phi_3}{\partial x_1} + [3(A_L L_L \rho_L + A_b L_b \rho_b + A_d L_d \rho_d)\right. \\ & \left. + m_p]\frac{\partial^2 u_{2,0}}{\partial t^2} - c_4 L_L\frac{\partial^2 u_{2,0}}{\partial x_1^2}\right)\delta u_{2,0} - 2\sqrt{3}L_b m_p\left(\delta u_{2,0}\frac{\partial^2 \phi_1}{\partial t^2}\right. \\ & \left.\left. - \delta u_{1,0}\frac{\partial^2 \phi_2}{\partial t^2} + \delta\phi_1\frac{\partial^2 u_{2,0}}{\partial t^2}\right)\right]\mathrm{d}x_1\,\mathrm{d}t \end{aligned} \tag{C1}$$

Because the variations for all of the coordinates of vibrations are arbitrary, we can assume that these variations are zero at the boundaries and, subsequently, the following relations are valid:

$$\int_0^t \int_0^{L_{\text{tot}}} \left(\phi_2 + \frac{\partial u_{3,0}}{\partial x}\right)\left(\delta\phi_2 + \delta\frac{\partial u_{3,0}}{\partial x}\right) \mathrm{d}x\,\mathrm{d}t$$
$$= \int_0^t \int_0^{L_{\text{tot}}} \left(\phi_2\delta\phi_2 - \frac{\partial^2 u_{3,0}}{\partial x^2}\delta u_{3,0} + \frac{\partial u_{3,0}}{\partial x}\delta\phi_2 - \frac{\partial\phi_2}{\partial x}\delta u_{3,0}\right) \mathrm{d}x\,\mathrm{d}t$$
$$\int_0^t \int_0^{L_{\text{tot}}} \left(\phi_3 - \frac{\partial u_{2,0}}{\partial x}\right)\left(\delta\phi_3 - \delta\frac{\partial u_{2,0}}{\partial x}\right) \mathrm{d}x\,\mathrm{d}t$$
$$= \int_0^t \int_0^{L_{\text{tot}}} \left(\phi_3\delta\phi_3 - \frac{\partial^2 u_{2,0}}{\partial x^2}\delta u_{2,0} - \frac{\partial u_{2,0}}{\partial x}\delta\phi_3 + \frac{\partial\phi_3}{\partial x}\delta u_{2,0}\right) \mathrm{d}x\,\mathrm{d}t$$
$$\int_0^t \int_0^{L_{\text{tot}}} \left(\delta\frac{\partial\phi_1}{\partial t}\frac{\partial u_{2,0}}{\partial t} + \frac{\partial\phi_1}{\partial t}\delta\frac{\partial u_{2,0}}{\partial t}\right) \mathrm{d}x\,\mathrm{d}t$$
$$= \int_0^t \int_0^{L_{\text{tot}}} \left(-\frac{\partial^2 u_{2,0}}{\partial t^2}\delta\phi_1 - \frac{\partial^2\phi_1}{\partial t^2}\delta u_{2,0}\right) \mathrm{d}x\,\mathrm{d}t$$

We can also write

$$\delta\left(\frac{\partial f}{\partial x}\right)\frac{\partial f}{\partial x} = -\delta f\frac{\partial^2 f}{\partial x^2}, \qquad \delta\left(\frac{\partial f}{\partial t}\right)\frac{\partial f}{\partial t} = -\delta f\frac{\partial^2 f}{\partial t^2} \tag{C2}$$

where f is each of the coordinates of vibrations Φ_1, Φ_2, Φ_3, $u_{1,0}$, $u_{2,0}$ and $u_{3,0}$. Making the substitution for Eq. (C2) into Equation (C1) results in a linear combination of the six equations of motion and, subsequently, Eqs. (12) and (13) can be found. The partial differential equations of motion for the plate model can be found in a similar manner.

Acknowledgments

This research was conducted at the Center for Intelligent Material Systems and Structures (CIMSS) at Virginia Polytechnic Institute and State University. This work was supported by the Defense Advanced Research Projects Agency (DARPA) through NASA Langley Research Center and the National Institute of Aerospace, for which we are grateful. The authors also thank Pablo Tarazaga at CIMSS, Virginia Polytechnic Institute and State University, for providing us with figures of the three-dimensional schematic of the innovative space based radar antenna technology.

References

[1] Chmielewski, A. B., "Overview of Gossamer Structures," *Gossamer Spacecraft: Membrane and Inflatable Structures Technology for Space Applications*, edited by, C. H. M. Jenkins, Vol. 191, Progress in Astronautics and Aeronautics, AIAA, Reston, VA, 2001, pp. 2–3.

[2] Sun, C. T., and Liebbe, S. W., "Global-Local Approach to Solving Vibration of Large Truss Structures," *AIAA Journal*, Vol. 28, No. 2, 1990, pp. 303–308.

[3] Salehian, A., Cliff, E. M., and Inman, D. J., "Continuum Modeling of an Innovative Space Based Radar Antenna Truss," *Journal of Aerospace Engineering*, Festschrift issue, Vol. 19, No. 4, 2006, 227–240.

[4] Yang, B., and Tan, C. A., "Transfer Functions of One-Dimensional Distributed Parameter Systems," *Journal of Applied Mechanics*, Vol. 59, No. 4, 1992, pp. 1009–1014.

[5] Heki, K., and Saka, T., "Stress Analysis of Lattice Plates as Anisotropic Continuum Plates," *Proceedings of the 1971 IASS Pacific Symposium, Part 2: Tension Structures and Space Frames*, Architectural Inst. of Japan, Tokyo, 1972, pp. 663–674.

[6] Noor, A. K., Greene, W. H., and Anderson, M. S., "Continuum Models for Static and Dynamic Analysis of Repetitive Lattices," *18th Structures, Structural Dynamics and Materials Conference*, AIAA, New York, 1977, pp. 299–310.

[7] Noor, A. K., Anderson, M. S., and Greene, W. H., "Continuum Models for Beam and Plate-Like Lattice Structures," *AIAA Journal*, Vol. 16, No. 12, 1978, pp. 1219–1228.

[8] Noor, A. K., and Andersen, C. M., "Analysis of Beamlike Lattice Trusses," *Computer Methods in Applied Mechanics and Engineering*, Vol. 20, No. 1, 1979, pp. 53–70.

[9] Noor, A. K., and Russell, W. C., "Anisotropic Continuum Models for Beamlike Lattice Trusses," *Computer Methods in Applied Mechanics and Engineering*, Vol. 57, No. 3, 1986, pp. 257–277.

[10] Nayfeh, A. H., and Hefzy, M. S., "Continuum Modeling of Three Dimensional Rod-Like Discrete Structures," *Proceedings of the International Symposium on Continuum Models of Discrete Systems*, University of Waterloo, Waterloo, Canada, 1977, pp. 339–357.

[11] Lake, M. S., and Kalng, E. C., "Generation and Comparison of Globally Isotropic Space-Filling Truss Structures," *AIAA Journal*, Vol. 30, No. 5, 1992, pp. 1416–1424.

[12] Sun, C. T., and Kim, B. J., "Continuum Modeling of Periodic Truss Structures," *Damage Mechanics and Continuum Modeling*, edited by N. Stubbs and D. Krajcinovic, American Society of Civil Engineers, New York, 1985, pp. 57–71.

[13] Lee, U., "Dynamic Continuum Plate Representations of Large Thin Lattice Structures," *AIAA Journal*, Vol. 31, No. 9, 1993, pp. 1734–1736.

[14] Lee, U., "Equivalent Continuum Representation of Lattice Beams: Spectral Element Approach," *Engineering Structures*, Vol. 20, No. 7, 1998, pp. 587–592.

[15] Burgart, B., and Cartraud, P., "Continuum Modeling of Beamlike Lattice Trusses Using Averaging Method," *Computers and Structures*, Vol. 73, Nos. 1–5, 1999, pp. 267–279.

[16] Tollenaere, H., and Caillerie, D., "Continuous Modeling of Lattice Structures by Homogenization," *Advances in Engineering Software*, Vol. 29, No. 7, 1989, pp. 699–705.

[17] Dean, D. L., and Avent, R. R., "State of the Art of Discrete Field Analysis of Space Structures," *Proceedings of the Second International Conference on Space Structures*, edited by W. J. Supple, Univ. of Guildford, Guildford, England, U.K., Sept. 1975, pp. 7–16.

[18] Wha, T., "Natural Frequencies of Uniform Grillages," *Journal of Applied Mechanics*, Vol. 30, No. 1, 1963, pp. 571–578.

[19] Wha, T., "Free Lateral Oscillations of a Supported Grillage," *Journal of the Franklin Institute*, Vol. 277, No. 4, 1964, pp. 349–360.

[20] GangaRao, H. V. S., and Smith, J. C., "Dynamic Field Analysis of Torsionless Grids," *Journal of Engineering Mechanics*, Vol. 98, No. 3, 1972, pp. 679–693.

B. Balachandran
Associate Editor